Durable immunogenicity, adaptation to emerging variants, and low-dose efficacy of an AAV-based COVID-19 vaccine platform in macaques

Nerea Zabaleta, Urja Bhatt, Cécile Hérate, Pauline Maisonnasse, Julio Sanmiguel, Cheikh Diop, Sofia Castore, Reynette Estelien, Dan Li, Nathalie Dereuddre-Bosquet, et al.

Molecular Therapy
Original Article

Durable immunogenicity, adaptation to emerging variants, and low-dose efficacy of an AAV-based COVID-19 vaccine platform in macaques

Nerea Zabaleta,[1,2,3,4,11] Urja Bhatt,[1,2,3,4,11] Cécile Hérate,[5,11] Pauline Maisonnasse,[5] Julio Sanmiguel,[1,2,3,4] Cheikh Diop,[1,2,3,4] Sofia Castore,[1,2,3,4] Reynette Estelien,[1,2,3,4] Dan Li,[1,2,3,4] Nathalie Dereuddre-Bosquet,[5] Mariangela Cavarelli,[5] Anne-Sophie Gallouët,[5] Quentin Pascal,[5] Thibaut Naninck,[5] Nidhal Kahlaoui,[5] Julien Lemaitre,[5] Francis Relouzat,[5] Giuseppe Ronzitti,[6] Hendrik Jan Thibaut,[7] Emanuele Montomoli,[8,9] James M. Wilson,[10] Roger Le Grand,[5,12] and Luk H. Vandenberghe[1,2,3,4,12]

[1]Grousbeck Gene Therapy Center, Schepens Eye Research Institute, Mass Eye and Ear, Boston, MA 02114, USA; [2]Ocular Genomics Institute, Department of Ophthalmology, Harvard Medical School, Boston, MA 02114, USA; [3]The Broad Institute of Harvard and MIT, Cambridge, MA 02142, USA; [4]Harvard Stem Cell Institute, Harvard University, Cambridge, MA 02138, USA; [5]Center for Immunology of Viral, Auto-immune, Hematological and Bacterial Diseases (IMVA-HB/IDMIT), Université Paris-Saclay, Inserm, CEA, 92260 Fontenay-aux-Roses, France; [6]Généthon INTEGRARE UMR-S951 (Institut National de la Santé et de la Recherche Médicale, Université d'Evry, Université Paris-Saclay), 91000 Evry, France; [7]KU Leuven Department of Microbiology, Immunology and Transplantation, Rega Institute, Translational Platform Virology and Chemotherapy (TPVC), 3000 Leuven, Belgium; [8]VisMederi Srl, 53100 Siena, Italy; [9]University of Siena, Department of Molecular Medicine, 53100 Siena, Italy; [10]Gene Therapy Program, Perelman School of Medicine, University of Pennsylvania, Philadelphia, PA 19104, USA

The COVID-19 pandemic continues to have devastating consequences on health and economy, even after the approval of safe and effective vaccines. Waning immunity, the emergence of variants of concern, breakthrough infections, and lack of global vaccine access and acceptance perpetuate the epidemic. Here, we demonstrate that a single injection of an adenoassociated virus (AAV)-based COVID-19 vaccine elicits at least 17-month-long neutralizing antibody responses in non-human primates at levels that were previously shown to protect from viral challenge. To improve the scalability of this durable vaccine candidate, we further optimized the vector design for greater potency at a reduced dose in mice and non-human primates. Finally, we show that the platform can be rapidly adapted to other variants of concern to robustly maintain immunogenicity and protect from challenge. In summary, we demonstrate this class of AAV can provide durable immunogenicity, provide protection at dose that is low and scalable, and be adapted readily to novel emerging vaccine antigens thus may provide a potent tool in the ongoing fight against severe acute respiratory syndrome coronavirus-2 (SARS-CoV-2).

INTRODUCTION

The coronavirus disease 2019 (COVID-19) pandemic continues to affect health and cause disruption. The approved vaccines have shown excellent safety and efficacy to prevent COVID-19, the disease caused by the severe acute respiratory syndrome coronavirus-2 (SARS-CoV-2).[1–4] As vaccination campaigns advanced, the risk of serious disease and death in the vaccinated was greatly reduced;[5] however, vaccine effectiveness declined due to waning immunity, particularly of mRNA-based vaccines.[6–8] The emergence of novel variants further exacerbates the risk for breakthrough infection. Lastly, studies suggest that, when vaccinated, transmission remains significant.[9]

These events overlaid the fact that a large proportion of the global population that remains unvaccinated, either by choice or by lack of access, continues to fuel the infection rate globally, resulting in an acceleration of the emergence of variants that are increasingly further removed from the ancestral SARS-CoV-2 strain. D614G was one of the first mutations to become globally prevalent and was found to be associated with increased viral load in the upper respiratory tract but not neutralization escape from antibodies generated against the parental Wuhan strain.[10–12] In December 2020 and January 2021, several neutralization escape variants of SARS-CoV-2 emerged in different locations with distinct mutations in the genome, most notably in the N-terminal domain (NTD), receptor binding domain (RBD), and near the furin cleavage site of the Spike protein, the main antigen in most COVID-19 vaccines.[13–17] The World Health Organization (WHO) classified these as variants of concern (VOCs), variants of interest (VOIs), and variants under monitoring (VUMs, or variants

Received 7 March 2022; accepted 7 May 2022;
https://doi.org/10.1016/j.ymthe.2022.05.007.

[11]These authors contributed equally

[12]These authors contributed equally

Correspondence: Luk H. Vandenberghe, PhD, Grousbeck Gene Therapy Center, Schepens Eye Research Institute, Mass Eye and Ear, Boston, MA 02114, USA
E-mail: luk_vandenberghe@meei.harvard.edu

being monitored [VBM]) (https://www.who.int/en/activities/tracking-SARS-CoV-2-variants/). The cross-reactivity of antibodies elicited by natural infection with the Wuhan parental strain or by vaccination with the approved Wuhan Spike-based vaccines has been shown to be less potent against some VOCs.[18–23] The Beta variant was shown to escape immunity to the ancestral variant significantly,[19,24] although potent antibody responses against Wuhan remain to confer protective immunity against Beta.[25,26] Many breakthrough infections have also been reported to be caused by Delta VOC, which emerged likely out of India in the summer of 2021.[27,28] In November 2021, the Omicron variant was first detected in South Africa and spread globally within a short month afterward. Remarkably, the Omicron Spike protein varies in more than 30 mutations compared with the ancestral Wuhan Spike and antigenically confers the greatest divergence, leading to profound immune escape in vaccinated and convalescent individuals.[29,30]

Compounding the threat of immune-escape SARS-CoV-2 variants, the immunity elicited by natural infection or by mRNA vaccines appears to wane within months after immunization. Indeed, antibody titers induced by mRNA-based vaccines progressively wane after two doses of immunization by as much as 10-fold in 6 months,[6–8] requiring a booster to recover protective immunity. Other vaccines, such as the single-shot Ad26, appear to perhaps provide more durable immunity, but overall demonstrate lower protection from disease and reduced antibody levels compared with mRNA at its peak efficacy.[31]

The emerging VOCs and the waning immunity in the vaccinated have prompted manufacturers and health authorities to recommend the need of a third dose as a booster. While mRNA manufacturers have developed and performed initial clinical studies on VOC-based COVID vaccines, immunity with VOC-adapted vaccine candidates is only modestly superior to boosting with the original Wuhan-strain-based vaccine.[32] To avoid extensive studies and timelines that authorization of a new vaccine candidate would require, the already-approved Wuhan-based mRNA vaccines have been recommended as boosters as they indeed induce potent cross-reactive responses.

While many second-generation vaccines are under development, their path to approval is complicated in light of the increasing safety database on the approved vaccines. However, given the limitations of current vaccines, particularly on the durability of mRNA, the emergence of VOCs, and the need for continued booster doses, further vaccine solutions are sought in this protracted epidemic.

We previously reported the preclinical efficacy of an adenoassociated virus (AAV)-based COVID-19 vaccine (AAVCOVID).[33] AAVCOVID candidates demonstrated durability of high neutralizing responses in non-human primate (NHP) models for at least 11 months following a single-dose immunization. In a separate SARS-CoV-2 study, these levels were shown to be highly protective in the upper and lower airways. AAVCOVID was leveraging established manufacturing capacity in the industry, which can be scaled. Last, studies indicated the vaccine product was stable for 1 month at room temperature. Here, we provide an update on the ongoing durability NHP study at approximately 20 months.

In addition, we sought to optimize the platform by reducing the dose requirement to maximize scalability and lower cost. We further illustrate the adaptability and robustness of the platform by incorporating several VOC-specific antigens on the platform vector at rapid pace and by maintaining overall potency. Here, we report protection data of the previously described AAVCOVID vaccine candidates at a lower dose in a macaque challenge model. Additionally, we have engineered AAVCOVID vectors and improved their potency by 10- to 40-fold in mouse and NHPs. We have also adapted our most potent vaccine to Beta, Delta, and Omicron VOCs, showing a fast and efficient adaptability of the platform. Finally, we have demonstrated that the optimized AAVCOVID candidates can confer protection against VOCs at lower doses.

RESULTS

AAVCOVID vaccines elicit durable immunogenicity in rhesus macaques

AC1 and AC3 vaccines were previously described and characterized in mouse models.[33] Briefly, AC1 expresses the full-length prefusion stabilized Wuhan Spike (Spp) under the control of an SV40 promoter and AC3 the secreted S1 subunit of Wuhan Spike under the control of a cytomegalovirus (CMV) promoter, and both are AAVrh32.33 capsid based. Previously, we reported that both candidates at high dose elicited durable (up to 11 months) neutralizing antibody responses in rhesus macaques (n = 2/candidate).[33] Figure 1A shows that the antibody response remains stable and at peak levels 20 months (week 88) after a single-dose administration. Figure 1B shows antibody titers in six cynomolgus macaques 9 weeks after being vaccinated with 10^{12} genome copies (gc) of AC1 (mimicking the vaccination regime in the rhesus animals described in Figure 1A), which were challenged with SARS-CoV-2 after week 9 and were shown to have near-sterilizing protective immunity.[33] Importantly, all four animals in Figure 1A presented neutralizing antibody titers in range with the titers observed in protective immunity (Figure 1B) at all timepoints measured from week 8 to week 70. This study is ongoing and intended for long-term follow-up of Spike neutralizing responses. Additionally, cross-reactivity with the better escape VOC variants (Beta, Delta, and Omicron) was measured (Figure 1C). Overall, titers decreased against Beta and Delta but remained detectable up to week 88, except in the AC3 animal with the lowest titers. As expected, neutralization of Omicron is greatly reduced in all animals, although three of them showed neutralization of Omicron in most of the timepoints analyzed (Figure 1C).

Low doses of first-generation AAVCOVID only partially protect cynomolgus macaques

Previously, we reported that a single intramuscular (i.m.) dose of 10^{12} gc AC1 confers near-sterilizing immunity against SARS-CoV-2 challenge in NHPs.[33] In order to enhance the scalability and reduce the cost in line with vaccine expectations, we sought to reduce the dose requirement of the platform while retaining seroconversion rates, immunogenicity, and protection qualities. Cynomolgus macaques (n = 6/group) were

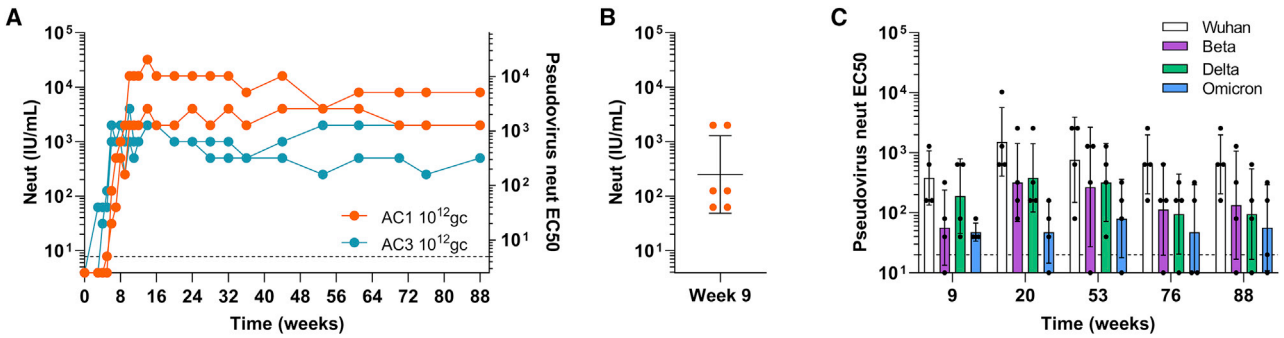

Figure 1. AAVCOVID vaccines elicit durable immunogenicity in macaques

(A) Longitudinal analysis of pseudovirus neutralization (international units [IU]/mL) in rhesus macaques vaccinated with 10^{12} genome copies (gc) of AC1 and AC3 (n = 2). (B) Pseudovirus neutralization (IU/mL) in cynomolgus macaques 9 weeks after vaccination with 10^{12} gc of AC1 and before SARS-CoV-2 challenge. (C) Longitudinal analysis of Beta, Delta, and Omicron VOC pseudovirus neutralization (reciprocal dilution) in rhesus macaques vaccinated with 10^{12} gc of AC1 and AC3 (n = 2). (B–C) Geometric mean ± SD.

therefore vaccinated with 10^{11} gc total of AC1 or AC3 vaccine candidates, and a third group was not vaccinated as a control. Antibody and T cell responses were followed for 9 weeks. All animals vaccinated with AC3 showed seroconversion of Wuhan RBD-binding and neutralizing antibodies by week 9 (Figures 2A, 2B, S1A, and S1B). AC1, however, failed to seroconvert all animals (Figure 2A) and neutralizing antibody titers were below the detection limits in most of them (Figure 2B). The same trends were observed in interferon gamma (IFN-γ) enzyme-linked immunosorbent spot (ELISpot) (Figure 2C).

All the animals were challenged with 10^5 plaque-forming units (PFU) of SARS-CoV-2 (BetaCoV/France/IDF/0372/2020).[34] This variant presents the differential V367F mutation compared with the B.1 ancestral strain. Vaccinated groups were partially protected from infection in the upper respiratory tract (Figures 2D and 2E). Three of six animals in the AC1 and AC3 groups presented detectable viral load (viral RNA and subgenomic RNA) in the nasal swabs, although the virus was cleared faster in the AC3 animals than in the controls (area under the curve [AUC] significantly smaller than controls), while the unprotected AC1 animals showed the same trend as controls (AUC statistically not different compared with controls). The remaining three animals in each group presented no viral load in the nasal swab, except for one animal in the AC1 group with a breakthrough in viral RNA on day 2. Similar observations were made in tracheal swabs (Figures S1C and S1D). Bronchoalveolar lavage (BAL) was also analyzed to assess protection of the lower respiratory tract. AC1 and AC3 cohorts showed trends to lower viral RNA in the lungs, although detectable, while subgenomic RNA was undetectable in all except one AC1 NHP (Figures 2F and 2G). This observation was confirmed by the analysis of lung lymph nodes by positron emission tomography (PET) scan (Figure 2H). Vaccinated animals did not show an activation of lymph nodes after challenge, which was observed in control animals, due to an active SARS-CoV-2 infection in the lungs (Figure 2H). Computed tomography (CT) scan did not reveal a significant difference in lung lesions due to the mild phenotype of SARS-CoV-2 infection in NHPs (Figure S1E). Lung histology analysis of vaccinated animals 30 to 35 days after challenge suggests fewer lesions due to COVID-19 infection in AC1 vaccinated animals, while no significant difference was observed between the scores of controls and AC3 vaccinated animals (Figure 2I).

Antibody responses after challenge increased in all the animals, including controls (Figures 2A, 2B, S1A, and S1B). Figure 2A illustrates that two of the animals treated with AC1 were non-responders, since the antibody levels after challenge followed the same trend as the unvaccinated and challenged controls. All AC3 animals, however, did seroconvert prior to the challenge, indicating that, at the 10^{11} gc level, the AAVCOVID platform can perform reliably.

Biodistribution was assessed for AC1 and AC3 at all doses tested (Figure S2A). Results show that AAVCOVID primarily biodistributes to the injected muscle, the regional lymph node, and spleen, while only minimal systemic biodistribution is observed in tissues like liver; at a dose of 10^{11} gc, approximately one vector genome per 10,000 diploid genomes is detected in any of the four liver lobes.

In summary, the AC1 and AC3 dose-reduction challenge studies indicated (1) that AC3 at the 10^{11} gc dose led to 100% seroconversion and a strong T cell response, yet was unable to achieve the previously demonstrated level of protection in the upper and lower airway as AC1 at the 10× higher dose,[33] and (2) that AC1 at the 10^{11} gc dose was unable to achieve full seroconversion, notwithstanding use of an identical viral vector capsid to AC3 carrying a superior antigen (full-length prefusion stable Spike compared with S1). The only remaining variable in the constructs between AC1 and AC3 were the regulatory regions of the promotor (SV40 in AC1 and CMV in AC3) and the polyadenylation sequences (SV40 in AC1 and a bovine growth hormone [bGH] in AC3).

Second-generation AAVCOVID platform is optimized for capsid and promoter

Based on the experience with AC1 and AC3 in the above studies and prior experiment,[33] we sought to further optimize the various characteristics of a broadly applicable vaccine platform: manufacturing,

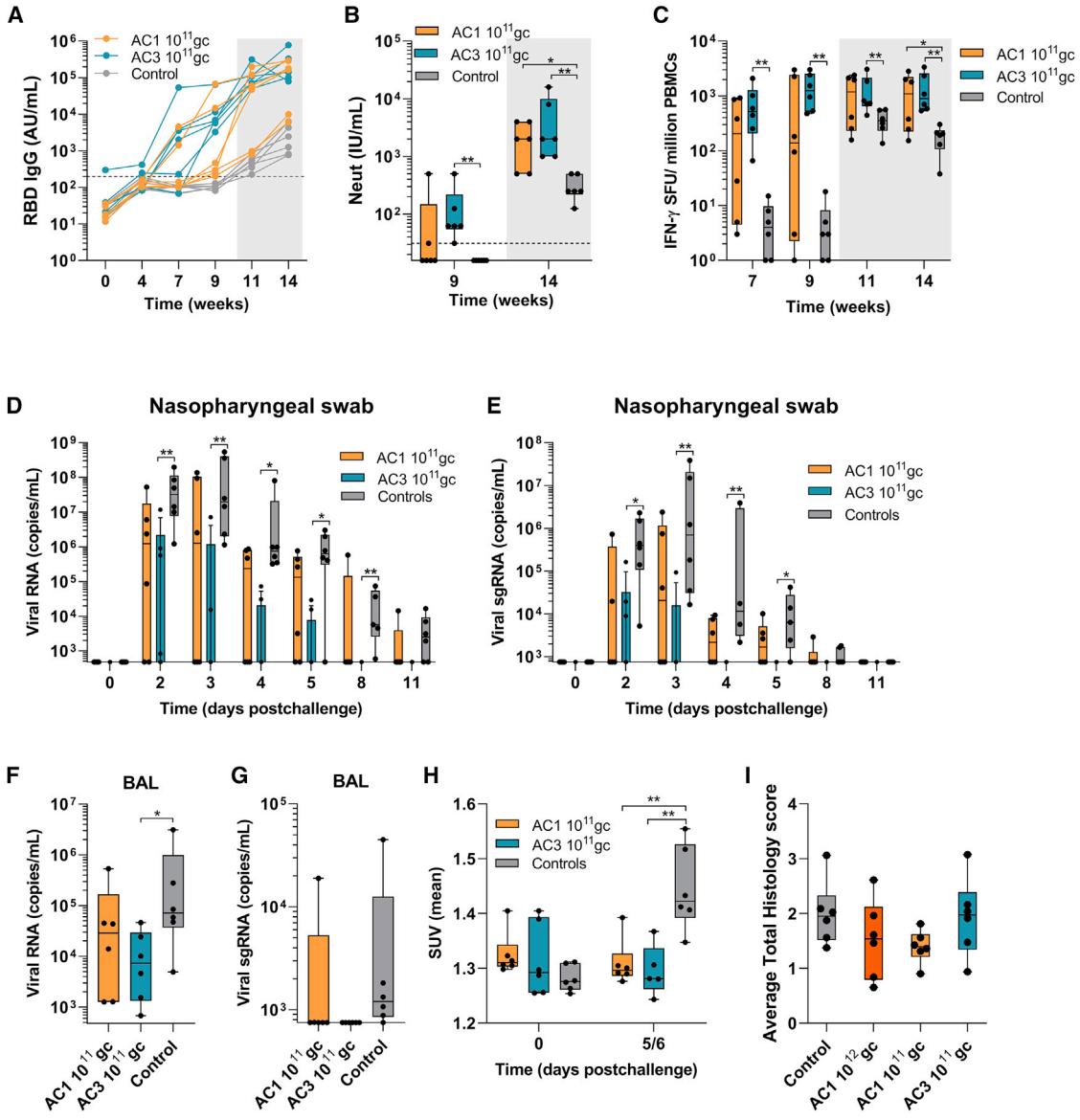

Figure 2. Low doses of first-generation AAVCOVID only partially protect cynomolgus macaques

Cynomolgus macaques vaccinated with 10^{11} gc of AC1 and AC3 (n = 6) and controls challenged with 10^5 PFU of SARS-CoV-2 (BetaCoV/France/IDF/0372/2020) on week 9.5 after vaccination. (A) RBD-binding IgG concentration (arbitrary units [AU]/mL). (B) Pseudovirus neutralization (IU/mL). (C) IFN-γ spot-forming units (SFU) per million PBMCs measured by ELISpot. SARS-CoV-2 viral RNA (D) and subgenomic RNA or sgRNA (E) quantification (copies/mL) after challenge in nasopharyngeal swabs. SARS-CoV-2 viral RNA (F) and sgRNA (G) quantification (copies/mL) 3 days after challenge in bronchoalveolar lavage (BAL). (H) Measurement of lung lymph node activation by PET as mean standardized uptake value (SUV mean) before and after challenge. (I) Lung histopathology score 30–35 days after challenge. (A–H) Mann-Whitney test was used to compare vaccinated groups with controls. *$p < 0.05$, **$p < 0.01$. Gray shaded areas correspond to post-challenge timepoints. (I) Tukey's test. ****$p < 0.0001$.

seroconversion, and potency of immunogenicity and protection at the lowest dose possible. We next explore optimizations of both vector capsid (mainly toward optimized and consistency of production) and potency (mainly toward dose reduction).

First, we evaluated the AAV11 serotype, a close homolog of AAVrh32.33. AAV11 is a natural serotype that was isolated from the liver of a cynomolgus monkey,[35] as opposed to the AAVrh32.33, which is man-made capsid and therefore more likely to suffer from structural deficits that hamper production and reduce yields.[36] From structural comparison with other known AAV serotypes, AAVrh32.33, AAV4, and AAV12 are the closest related serotypes to AAV11.[37] The VP1 sequence of AAV11 and AAVrh32.33 are 99.7% homologous with two amino acid difference (K167R and T259S in AAV11).

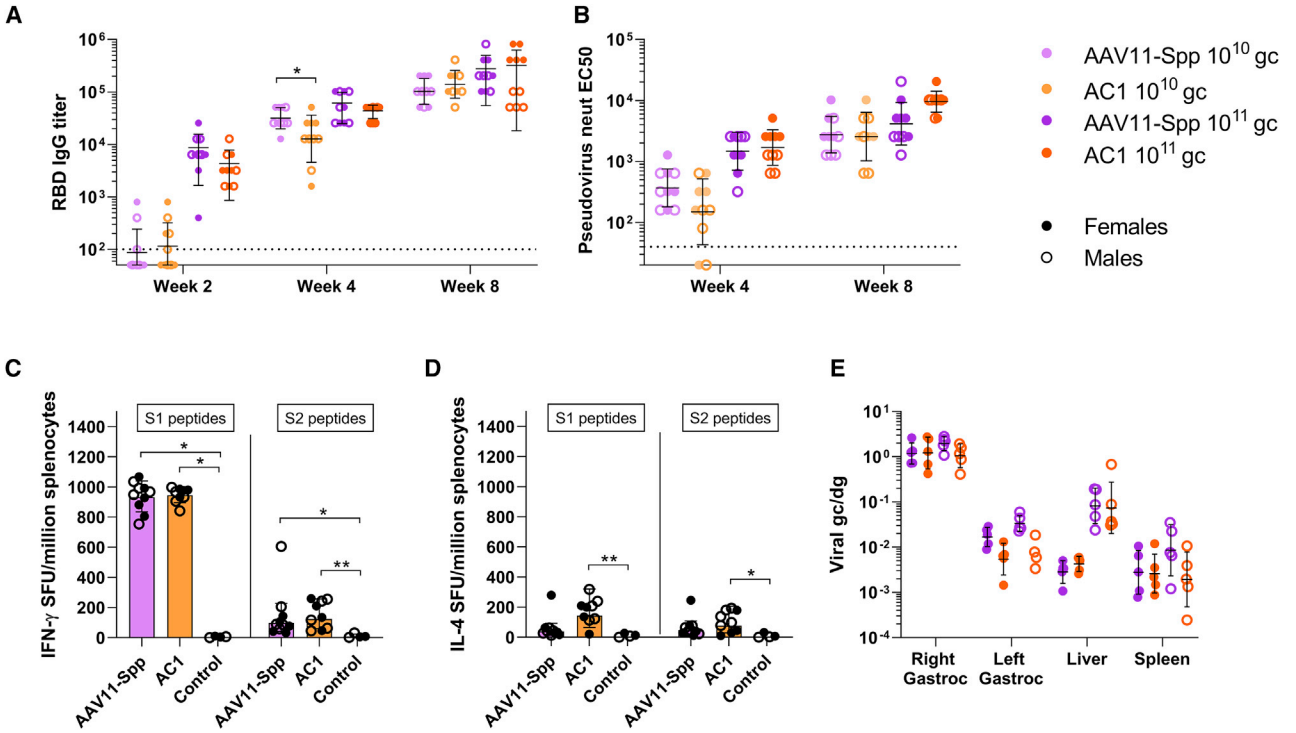

Figure 3. Second-generation AAVCOVID platform is optimized for capsid

C57BL/6 mice (7–8 weeks old) were injected i.m. with two doses (10^{10} gc and 10^{11} gc) of AC1 or AAV11-Spp, n = 10, five per gender). (A) SARS-CoV-2 RBD-binding IgG titers (reciprocal serum dilution). (B) Pseudovirus neutralizing titers (reciprocal serum dilution). SFU detected by IFN-γ (C) or IL-4 (D) ELISpot in splenocytes harvested 10 weeks after vaccination with 10^{10} gc of AC1 or AAV11-Spp and stimulated with Spike peptides. (E) Quantification of vector genome copies (genome copies/diploid genome [gc/dg]) in the right gastrocnemius (right gastroc) or injection site, left gastrocnemius (left gastroc) or contralateral muscle, liver, and spleen on week 10 (n = 5). The dotted lines indicate the lower detection limit of the assays. Data are represented as geometric mean ± SD. Unpaired t test with Welch's correction was used for comparison of animals with same dose of AAV11-Spp and AC1.

To ensure the vaccine properties of AAVrh32.33 were retained, AAV11 vectors containing the same cassette as AC1 (SV40 promoter expressing Spp) were produced and tested in mouse immunogenicity studies. Six- to 8-weeks-old male and female C57BL/6 mice were given 10^{11} and 10^{10} gc doses of AAV11-Spp vaccine and compared with an AAVrh32.33-based AC1 candidate. Spike binding and neutralizing responses were similar between mice vaccinated with AC1 and AAV11-Spp across doses and genders (Figures 3A and 3B). Cellular responses to the transgene were also preserved for the AAV11-based candidate, with robust IFN-γ responses against Spike peptides, mainly subunit 1 (S1) peptides and very low interleukin (IL)-4 secretion (Figures 3C and 3D). The biodistribution pattern of the vectors was analyzed on day 7 after i.m. administration, and the same distribution profiles were observed for AAVrh32.33 and AAV11 with most vector copies in the injected muscle (right gastrocnemius) (Figure 3E). The same results were observed in BALB/c mice injected with these vectors (Figure S3). AAV11 was the serotype used for all subsequent studies.

Based on the observations in the NHP dose-reduction studies in Figure 2, we hypothesized that increasing promoter strength would further optimize the immunogenicity of the AAVCOVID platform. This was further supported by expression data in C57BL/6 that previously demonstrated the CMV-driven antigen expression from AC3 was far greater than the SV40 expression in AC1.[33] We thus designed AAV expression cassettes to improve the expression of Spp. Spp was chosen as an antigen over S1 as prior studies in mice clearly indicated its superiority for generating neutralizing responses to SARS-CoV-2 and similar antigen designs in the currently US Food and Drug Administration (FDA)-approved vaccines have been highly efficacious and safe in large populations.[1–4]

However, the main limitation to including variations of regulatory elements (minimally, promoter and polyadenylation signal or polyA) is the packaging size limitation of the recombinant AAV genome: the open reading frame [ORF] of SARS-CoV-2 Spike is 3.8 Kb, which leaves less than 700 bp of space. The SV40 polyA in AC1 was substituted by a shorter synthetic polyA (SPA) to create AC1-SPA vector (Figure 4A). To increase the expression of Spike, the SV40 promoter was substituted by a short EF1α promoter (EFS), a minimal CMV promoter (miniCMV), or the full CMV promoter to create ACE1, ACM1, and ACC1 vectors, respectively (Figures 4A and S4A). The ACC1 promoter, due to the long size of the promoter, resulted in an oversized recombinant genome, which could lead to

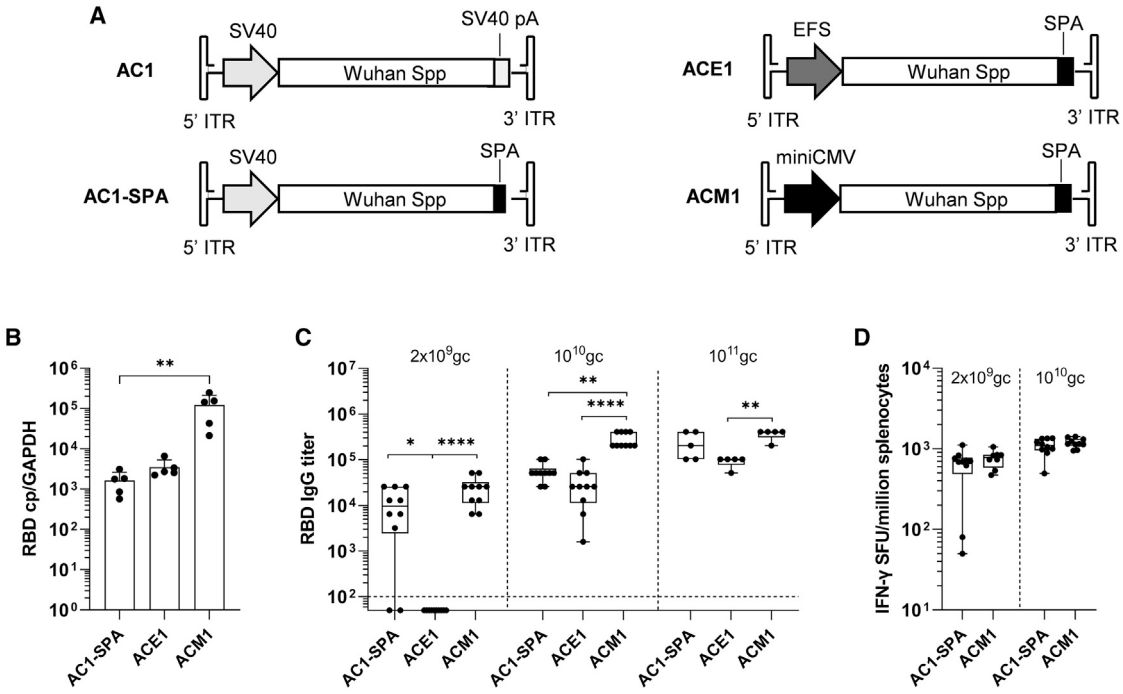

Figure 4. Second-generation AAVCOVID platform is optimized for promoter

(A) Scheme of new cassettes. SV40, simian virus 40 promoter and polyadenylation signal; ITR, inverted terminal repeat; Spp, prefusion stabilized Spike; SPA, synthetic polyA; EFS, elongation factor short promoter; miniCMV, minimal CMV promoter. (B) Transgene mRNA expression (RBD copies [cp]/GAPDH copies) 7 days after i.m. administration of 10^{11} gc in C57BL/6 animals (n = 5 females). Data are represented as mean ± SD. (C) RBD-binding antibody titers in C57BL/6 animals (n = 5–10 females) at three different doses. (D) IFN-γ ELISpot on day 56 after vector administration. (A and B) Kruskal Wallis test and Dunn's posttest. (C) Mann-Whitney test. *p < 0.05, **p < 0.01, ****p < 0.0001.

fragmented genome packaging and lower vector yields at scale.[38,39] *In vitro* expression studies revealed improved expression of Spike protein in cells infected with ACM1 and ACC1 compared with AC1 (Figure S4B). This was confirmed in C57BL/6 female animals that received these candidates by measuring Spike mRNA levels in the injected muscle 7 days after a 10^{11} gc i.m. injection (Figures 4B and S4C). Higher expression resulted in significantly higher RBD-binding antibody levels in animals vaccinated with ACM1 compared with AC1-SPA and ACE1 at three doses ranging from 2×10^9 gc to 10^{11} gc. Interestingly, ACM1 achieved full seroconversion with a single dose as low as 2×10^9 gc per mouse, while 20% of AC1-SPA animals at the same dose were found to be non-responders by analyzing humoral and cellular immune responses (Figures 4C and 4D). No significant difference was found in IFN-γ ELISpot between AC1-SPA and ACM1 (Figure 4D). ACC1 also showed increased transduction in the injected muscle and increased antibody responses, in line with ACM1 (Figures S4C and S4D).

ACM-Beta protects from Beta SARS-CoV-2 challenge in cynomolgus macaques at low dose

To further validate the efficacy of ACM compared with AC at the low 10^{11} gc dose, we performed a cynomolgus study in which animals were challenged with SARS-CoV-2. An ACM vector was generated expressing the Beta strain of SARS-CoV-2.

Cynomolgus macaques (n = 5) were i.m. injected with ACM-Beta and challenged at 7 weeks following the single dose vaccination. Immunogenicity was analyzed at various timepoints before and following the viral challenge. All animals seroconverted by week 6 (in contrast to AC1 at the same dose), as measured by Beta RBD-binding antibodies (Figures 2A and 5A). ACE2-binding inhibition assay and pseudovirus neutralization assay demonstrated similar efficiency but with modestly delayed kinetics, in line with the experience with AC1 or AC3[33] (Figures 5B and 5C). IFN-γ-mediated cellular responses as measured by ELISpot on peripheral blood mononuclear cells (PBMCs) were elevated by week 4 (Figure 5D). Cross-neutralization was measured by RBD-binding, ACE2 inhibition, and pseudovirus assay (Figure S5). Binding antibody levels were very similar for different VOC RBDs (Figure S5A), but ACE2 inhibition and pseudovirus neutralization were superior for Beta and Gamma variants compared with for Wuhan, Alpha, and Delta (Figures S5B and S5C).

The viral challenge consisted of an intranasal and intratracheal instillation of 10^5 PFU of Beta SARS-CoV-2 VOC (isolate hCoV-19/USA/MD-HP01542/2021, lineage B.1.351). Viral and subgenomic RNA were measured in the upper and lower respiratory tracts at various timepoints before and after challenge. In some vaccinated animals, viral RNA was detected in nasopharyngeal and tracheal swabs, as well as in the BAL harvested on day 3 after inoculation of the virus

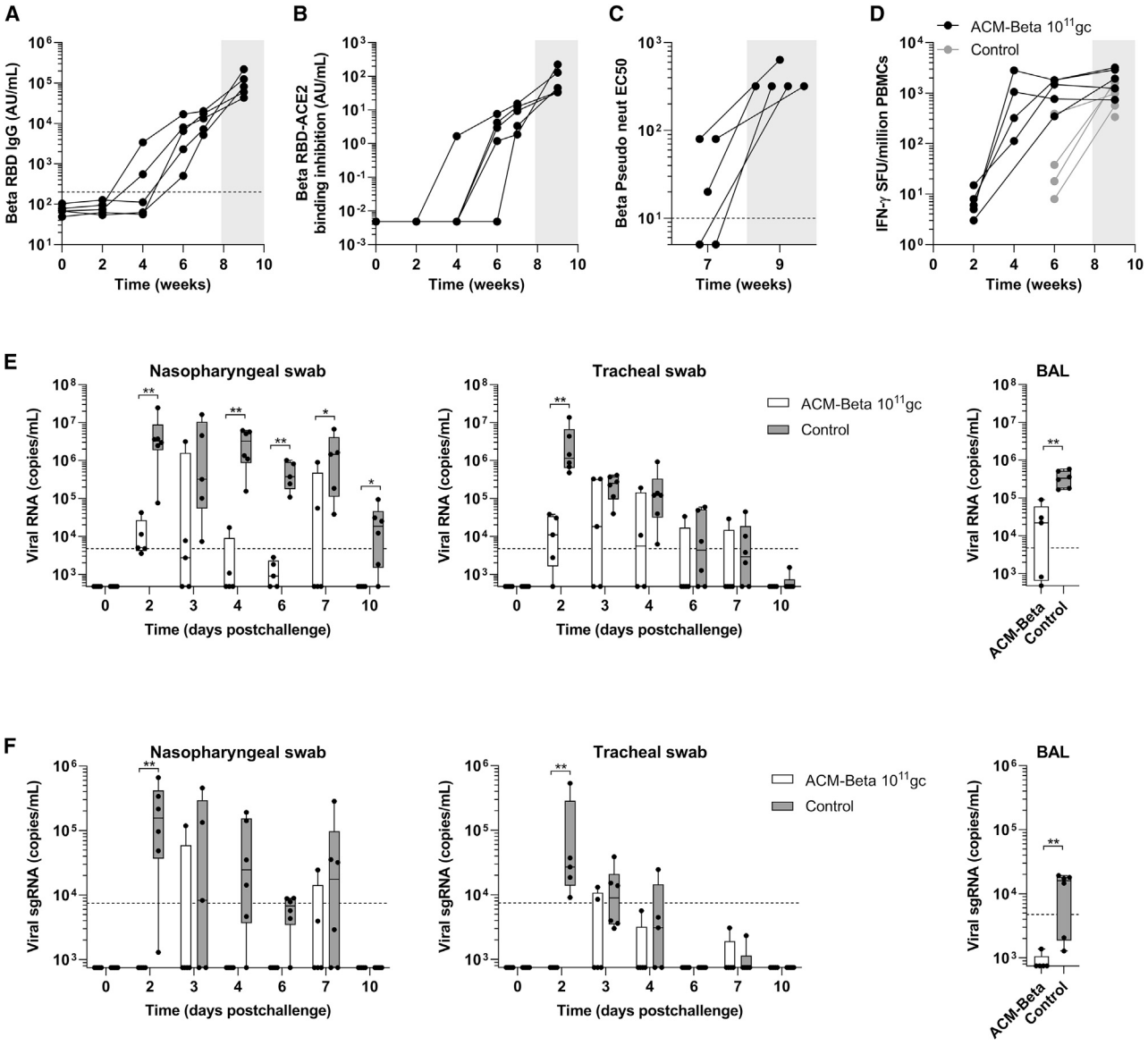

Figure 5. ACM-Beta protects from Beta SARS-CoV-2 challenge in cynomolgus macaques at low dose

Cynomolgus macaques vaccinated with 10^{11} gc of ACM-Beta (n = 5) and controls (n = 6) challenged with 10^5 PFU of Beta SARS-CoV-2 VOC on week 7.5 after vaccination. (A) Beta RBD-binding IgG concentration (AU/mL) in vaccinated animals. (B) ACE2 binding inhibition assay (AU/mL) in vaccinated animals. (C) Beta Spike pseudovirus neutralizing antibody titer (EC50) in vaccinated animals. (D) IFN-γ SFU per million PBMCs measured by ELISpot. Beta SARS-CoV-2 viral RNA (E) and subgenomic RNA or sgRNA (F) quantification (copies/mL) after challenge in nasopharyngeal swabs and tracheal swabs during 10 days after the challenge and in bronchoalveolar lavage (BAL) on day 3. Mann-Whitney test. *$p < 0.05$, **$p < 0.01$.

(Figure 5E). Overall viral loads were significantly lower (significantly lower AUC in both nasopharyngeal and tracheal viral RNA) and were cleared faster. Regarding active replication of the virus, only one animal presented single guide RNA (sgRNA) detectable above the limit of quantification on day 3 (Figure 5F). sgRNA was not detectable in BAL samples on day 3 (Figure 5F). These data demonstrated a protective effect from infection of ACM-Beta from SARS-CoV-2 Beta infection.

Biodistribution of the ACM-Beta vector was found to be consistent with AC1 at the same dose, primarily directed to the injected muscle, draining lymph node, and spleen. Systemic biodistribution was minimal (Figure S2B).

AAVCOVID induces polyfunctional CD4⁺ T cell responses

Cellular responses were measured in both NHP studies: (1) in animals vaccinated with 10^{12} and 10^{11} gc of AC1 and 10^{11} gc of AC3 on week 9

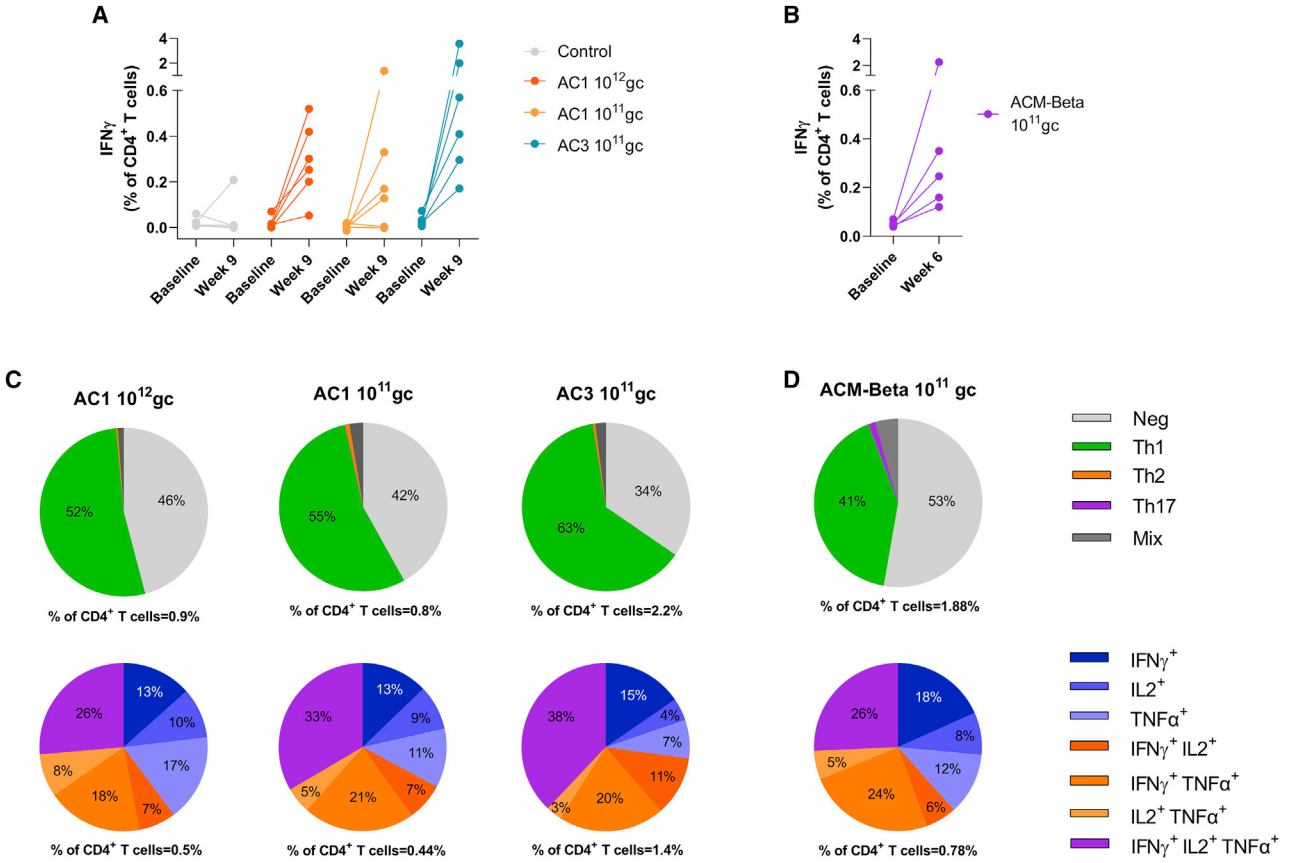

Figure 6. AAVCOVID induces potent CD4⁺ T cell responses

ICS analysis of PBMCs extracted from cynomolgus macaques vaccinated with first- and second-generation AAVCOVID vaccines on weeks 9 and 6, respectively. IFN-γ-secreting CD4+ T cells before and after vaccination in animals vaccinated with two doses of AC1 (A) (n = 6 per group), low dose of AC3 (A) (n = 6), and ACM-Beta (B) (n = 5). Pie charts showing the percentage of Th1 (IFN-γ, IL-2, and/pr TNF-α), Th2 (IL-13), and Th17 (IL-17)-specific cytokine-secreting CD4⁺ T cells (upper row) and percentage of Th1 cells secreting one, two, or three cytokines (lower row) on week 9 (C) and week 6 (D).

after vaccination, and (2) animals vaccinated with 10^{11} gc of ACM-Beta in PBMCs extracted on week 6. All animals developed IFN-γ-secreting CD4⁺ T cells, except the two animals in the AC1 low dose that failed to seroconvert after vaccination (Figures 6A and 6B). Upon stimulation with Spike peptides, percentages ranging from 0.8% to 2.2% of activated CD4+ T cells were detected by intracellular staining (ICS), and 41%–63% of these activated cells presented a Th1 phenotype (secretion of IFN-γ, IL-2, and/or tumor necrosis factor alpha [TNF-α]) (Figures 6C and 6D). From 26% to 38% of these Th1 phenotype cells were polyfunctional (secretion of the three cytokines), and around a third secreted combinations of two cytokines (Figures 6C and 6D). CD8 responses were mainly IFN-γ mediated (Figure S6). These data demonstrate that AAVCOVID elicited a robust and polyfunctional cellular response.

Robust and rapid programmability of ACM with VOC antigen

Gene-based vaccines can be designed and developed more quickly to respond to epidemic threats or the emergence of novel pathogenic strains (e.g., VOCs in the case of COVID-19). The responsiveness of the gene-based platforms such as mRNA is primarily due to the DNA-based template (e.g., plasmid DNA) as a substrate for the production process and the generic nature of the production and purification process independent of the encoded antigen. This is in contrast to other vaccine approaches that require viral or recombinant protein production, which is slower and specific to even subtle changes of the antigen.

AAV-based vaccines indeed rely on a plasmid-based substrate to initiate production that can be generated within days following the emergence and sequencing of a novel pathogen. Its production and purification are dependent on the viral capsid, which is kept consistent using the ACM platform. Indeed, in response to the Wuhan, Beta, Delta, and Omicron VOCs, ACM vectors specific to each VOC were developed and tested *in vivo* for immunogenicity, as illustrated in Figure 7. First, the SARS-CoV-2 Beta VOC is reported to be highly antigenically distinct from other variants, and hence is significantly less neutralized in individuals exposed to or immunized with the ancestral Wuhan Spike. Interestingly, however, individuals

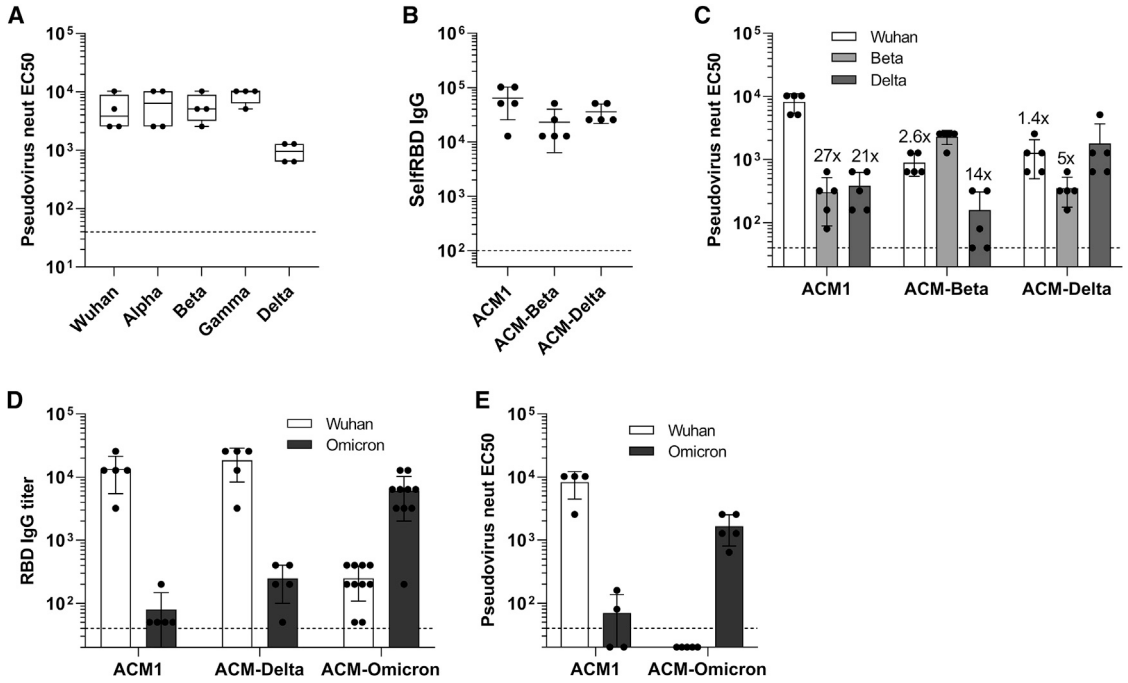

Figure 7. Robust and rapid programmability of ACM with VOC antigen

(A) VOC pseudovirus neutralization on day 56 in C57BL/6 animals vaccinated with 10^{11} gc of ACM-Beta (n = 4). (B) Self-RBD-binding antibody titers on day 14 in C57BL/6 animals vaccinated with 10^{11} gc of ACM1, ACM-Beta, or ACM-Delta (n = 5). (C) Different pseudovirus (Wuhan, Beta, and Delta) neutralization in animals vaccinated with different candidates on day 28 after vaccination (n = 5). (D) Wuhan and Omicron RBD-binding IgG titer in animals vaccinated with 10^{11} gc of ACM1, ACM-Delta, and ACM-Omicron on day 12. (E) Neutralization of Wuhan and Omicron pseudoviruses in animals vaccinated with 10^{11} gc of ACM1 and ACM-Omicron on day 28.

infected with Beta may develop stronger cross-reactivity to Wuhan and most of the other VOCs.[40] Indeed, C57/BL6 mice also developed high titers of neutralizing antibodies against Wuhan, Alpha, and Gamma VOCs following immunization with ACM-Beta compared with the neutralization potency to the Beta VOC itself (Figure 7A). In line with prior observations, cross-neutralization was lower for the Delta VOC.[41]

Next, we sought to evaluate the consistency of performance in terms of immunogenicity of the ACM platform in the context of Wuhan, Beta, and Delta Spike antigens. Figures 7B and 7C illustrate that both binding and neutralizing antibody titers are analogous for each of these vaccine candidates. VOC cross-reactivity of each of these vaccine responses was interrogated and illustrates their unique antigenic profile (Figure 7C). A separate more recent study included ACM-Omicron encoding the Omicron Spp demonstrating similar potency to ACM-1 and ACM-Delta in mice 12 days after vaccination (Figure 7D). Interestingly, cross-reactivity between Wuhan and Omicron (Figure 7D) is greatly reduced compared with Wuhan and Beta binding immunoglobulin G (IgG) antibody (Figure S7). The same trend was observed in cross-neutralizing antibody titers (Figure 7E).

DISCUSSION

The constantly evolving COVID-19 pandemic requires vaccines and vaccine regimens to adapt to the rapidly changing threat. Past experience demonstrates that vaccines are indeed a key tool in managing the ongoing crisis. However, for vaccines to eventually suppress the epidemic, that tool may need to be sharpened; rapid global deployment is needed to prevent the emergence of new variants; vaccines need to have breadth and/or adaptability to be effective against current and future VOCs; and protection from disease needs to be durable, and ideally also prevent transmission. Here, we evaluate and optimize an AAV-based COVID-19 vaccine platform in its potential to address some of the limitations that have been exposed.

Previously, we demonstrated proof-of-concept data that a first-generation AAVCOVID candidate can fully suppress viral replication in the upper and lower respiratory tract and confer protection against SARS-CoV-2 challenge in NHPs at a single 10^{12} gc dose.[33] Here we show that this generation of the AAV-based vaccine technology in the context of COVID-19 leads to sustained neutralizing antibody production for at least 20 months at plateau levels that studies indicate to be protective in NHPs, on par with mRNA levels following a two-dose prime regimen and convalescence of an intensive care unit (ICU) cohort in humans. We further demonstrated previously that this AAV-based vaccine product is high yielding in production and was adapted to a scalable manufacturing process. The vaccine product was found to be stable when stored for 1 month at room temperature and at least 12 weeks at 4°C in a simple modified saline buffer.

These preclinical data, if recapitulated in human subjects, suggest that the profile of AAVCOVID may overcome some of the limitations of currently approved COVID-19 vaccines (e.g. durable immunogenicity from a single dose, improved storage stability, potential for strong upper airway protection). As articulated by Dr. Fauci and colleagues most recently,[42] there is a continued need to fight epidemics, and specifically future coronavirus outbreaks, by accelerating the development of improved vaccine technologies specifically on attributes AAVCOVID may hold based on the presented data.

However, for this technology to be further considered toward clinical translation, several outstanding concerns warrant addressing that speak to safety, efficacy in humans, and feasibility. The studies presented here specifically sought to improve on potency for a lower dose to be sufficiently robust in terms of seroconversion and level of immunogenicity. A target of 10^{11} gc was established based on models to attain feasibility for scaled production and sufficiently low production cost in line with vaccine applications.

Dose-reduction viral challenge studies established that the first-generation candidates AC1 and AC3 do not meet that criterion; at 10^{11} gc, they were found insufficiently protective in a cynomolgus macaque SARS-CoV-2 challenge model. AC1 only partly seroconverted, while AC3 did seroconvert fully, but both vaccine candidates left several animals without evidence of protection from the viral challenge. Based on the available mouse and NHP expression, immunogenicity, and efficacy data, we were able to redesign the vaccine platform. By correlating AC1 and AC3 relative performance vis à vis their distinct design features, we hypothesized that increasing antigen expression would permit a potency increase and a dose reduction. However, due to size constraints, the CMV promoter used in AC3 could not be transferred to AC1. Therefore, we designed a construct with a minimal CMV promoter to achieve higher expression within the packaging limitation of AAV to drive the prefusion stable full-length SARS-CoV-2 Spike antigen. Additionally, the polyadenylation sequence was modified, although its impact on dose and potency was not fully established.

ACM vaccine candidates were produced and tested in murine models for the ancestral Wuhan SARS-CoV-2 strain, as well as the Beta, Delta, and Omicron VOCs. To assess any improvement of NHP efficacy at a lower dose, ACM-Beta was tested in a SARS-CoV-2 Beta viral challenge in cynomolgus macaques, illustrating strong protection at the reduced dose. Compared with prior protection data from AC1, however, some breakthrough viral replication was observed in nasal and tracheal swabs. Further studies are needed to identify whether this is indicative of a lower potency of the vaccine candidate at this lower dose, or perhaps due to the shorter timing between immunization and challenge (7 versus 9 weeks) comparing both studies. The kinetics of antibody induction in NHPs (Figure 1) indicate a potential 100× increase over those 2 weeks, which may indeed further strengthen the level of protection observed in the current study. Last, T cell responses from AC and ACM were strong and polyfunctional at all of the doses tested.

In summary, AAV-based vaccines for COVID-19 can be effective from a single, low dose and lead to durable humoral and strong T cell immunogenicity. The storage conditions of AAVCOVID may allow for increased access and facile deployment. Further preclinical and clinical studies are needed to further bolster its safety profile and efficacy in humans.

Limitations of the study

Viral vector-based vaccines, such as AAVCOVID and adenovirus-based vaccines, elicit immunogenicity against the vector capsid, which may neutralize vector in subsequent administrations (e.g., in the context of a vaccine boost). Ongoing studies seek to evaluate AAVCOVID in the context of homologous and heterologous prime-boost strategies. While no safety concerns were noted in any of the studies supporting AAVCOVID, formal preclinical and clinical safety studies are needed. While our work supports the potential to scale AAV-based vaccines at vaccine-appropriate cost based on current-day processes and yield assumptions, process development and scaled manufacturing remain to be developed.

MATERIALS AND METHODS

NHP studies

Rhesus (*Macaca mulatta*) animal study was performed by University of Pennsylvania under the approval of the Institutional Animal Care and Use Committee of the Children's Hospital of Philadelphia. Rhesus macaques that screened negative for viral pathogens, including simian immunodeficiency virus (SIV), simian T-lymphotrophic virus (STLV), simian retrovirus (SRV), and B virus (macacine herpesvirus 1) were enrolled on the study. Animals were housed in an Association for Assessment and Accreditation of Laboratory Animal Care (AAALAC) International-accredited non-human primate research in stainless-steel squeeze-back cages, on a 12-h timed light/dark cycle, at temperatures ranging from 18°C to 26°C (64°F –79°F). Animals received varied enrichment such as food treats, visual and auditory stimuli, manipulatives, and social interactions throughout the study. Four 3- to 7-year-old rhesus macaques (*M. mulatta*) were treated with the clinical candidates (n = 2/vector, one female and one male) i.m. at a dose of 10^{12} gc/animal. Serum was obtained in regular intervals for several analyses of immunogenicity against SARS-CoV-2 Spike.

Cynomolgus macaques (*Macaca fascicularis*) aged 33-48 months (15 females and 12 males) and originally from Mauritian AAALAC-certified breeding centers were used for SARS-CoV-2 challenge studies. All animals were housed in Infectious Disease Models and Innovative Therapies (IDMIT) facilities (CEA, Fontenay-aux-Roses), under BSL-3 containment (animal facility authorization #D92-032-02, Préfecture des Hauts de Seine, France) and in compliance with European Directive 2010/63/EU, the French regulations, and the Standards for Human Care and Use of Laboratory Animals of the Office for Laboratory Animal Welfare (OLAW, assurance number #A5826-01, US). The protocols were approved by the institutional ethical committee Comité d'Ethique en Expérimentation Animale du Commissariat à l'Energie Atomique et aux Energies Alternatives (CEtEA #44) under statement number A20-037. The study was authorized by the

Research, Innovation and Education Ministry under registration number APAFIS#24434-2020030216532863 and APAFIS#28946-2021011312169043.

Cynomolgus macaques were randomly assigned to the experimental groups.

For the first study testing AC1 and AC3, the different vaccinated groups (n = 6 for each) received a 10^{12} gc or 10^{11} gc of AC1 vaccine candidate or 10^{11} gc of AC3 vaccine candidate, while control animals (n = 6) received only the diluent. Blood was sampled from vaccinated animals at weeks 0, 1, 2, 4, 5, 6, 7, 8, and 9. Sixty-seven days after immunization, all animals were exposed to a total dose of 10^5 PFU of SARS-CoV-2 virus (human coronavirus 2019 [hCoV-19]/France/lDF0372/2020 strain; GISAID EpiCoV platform under accession number EPI_ISL_406596) via the combination of intranasal and intratracheal routes (0.25 mL in each nostril and 4.5 mL in the trachea; i.e., a total of 5 mL; day 0), using atropine (0.04 mg/kg) for pre-medication and ketamine (5 mg/kg) with medetomidine (0.05 mg/kg) for anesthesia. Nasopharyngeal and tracheal swabs were collected at 2, 3, 4, 5, 8, 11, 14, and 25 days post exposure (d.p.e.), while blood was taken at 2, 3, 4, 5, 8, 11, 14, 25, and 31 d.p.e. Bronchoalveolar lavages (BALs) were performed using 50 mL of sterile saline at 3 and 11 d.p.e. PET-CT scans were performed at day 5 or 6 and a CT scan was done at day 14.

For the second study evaluating the ACM-Beta vaccine candidate, the vaccinated group (n = 5) received a 10^{11} gc of ACM-Beta vaccine candidate, while control animals (n = 6) received only diluent. Blood was sampled from vaccinated animals at weeks 0, 1, 2, 4, 5, 6, and 7. Fifty-four days after immunization, all animals were exposed to a total dose of 10^5 PFU of Beta SARS-CoV-2 VOC (isolate hCoV-19/USA/MD-HP01542/2021, lineage B.1.351) as described above. Nasopharyngeal and tracheal swabs were collected at 2, 3, 4, 6, 7, 10, and 14 d.p.e., while blood was taken at 2, 3, 4, 7, 10, and 14 days. BALs were performed using 50 mL of sterile saline at 3 and 11 d.p.e. CT scans were performed at day 3 and day 7 to quantify lung lesions.

Blood cell counts, hemoglobin, and hematocrit were determined from EDTA blood using a DXH800 analyzer (Beckman Coulter).

Mouse studies

Mouse studies and protocols were approved by the Schepens Eye Research Institute IACUC. C57BL/6 and BALB/c mice were injected i.m. in the right gastrocnemius with different doses of vaccine candidates. Blood was harvested by submandibular bleeds and serum isolated. Several tissues were harvested at necropsy for splenocyte extraction and for biodistribution and transgene expression analyses.

Vaccine candidates

First-generation AAVCOVID candidates were described and characterized previously.[33] Second-generation candidates (ACM1, ACM-Beta, and ACM-Delta) consist of the AAV11 vector that expresses the codon optimized, prefusion stabilized (furin cleavage site mutated to $G_{682}SAS_{685}$ and $P_{986}P_{987}$ substitutions), full-length SARS-CoV-2 Spike protein (Wuhan, Beta, and Delta Spike) under the control of a minimal CMV promoter and a small synthetic polyA. Vectors were produced as previously described.[33]

In vitro infection and Spike expression by western blot

5×10^4 HuH7 cell/well were seeded in 12-well plates and incubated overnight at 37°C. On the following day, cells were pre-incubated for 2 h with adenovirus 5 (Ad5) at an MOI of 20 PFU/cell, and infected with an MOI of 5×10^5 of AC1 or AC3. Cells were harvested 72 h later and lysed with NuPAGE LDS Sample Buffer (4×) (Thermo Fisher Scientific, catalog no. NP0007) at 99°C for 5 min. Proteins were separated by electrophoresis in NuPAGE 4%–12% polyacrylamide gels (Thermo Fisher Scientific, catalog no. NP0321PK2) and then transferred to polyvinylidene fluoride (PVDF) membranes. The membranes were probed with an anti-SARS-CoV-2 RBD rabbit polyclonal antibody (Sino Biological, 40592-T62) followed by a goat anti-rabbit horseradish peroxidase (HRP)-conjugated secondary antibody (Thermo Fisher Scientific, catalog no. A16110, RRID: AB_2534782). Membranes were developed by chemiluminescence using the Immobilon Western Chemiluminescent HRP Substrate (Millipore, catalog no. WBKLS0500) and recorded using ChemiDoc MP Imaging System (Bio-Rad). An anti-GAPDH antibody (Cell Signaling Technology, catalog no. 2118, RRID: AB_561053) was used as loading control.

Quantification of antibodies by mesoscale

Cynomolgus macaque samples were screened for Spike and RBD-specific IgG and their neutralizing capacity (analyzed by a pseudo-neutralizing Spike-ACE2 assay) against SARS-CoV-2 wild-type and variants B.1.1.7, B.1.351, and P.1 using the V-PLEX SARS-CoV-2 Panel 7 (IgG and ACE2, MesoScale Discovery [MSD], Rockville, USA) according to the manufacturer's instructions and as previously described.[43] The plates were blocked with 50 µL of blocker A (1% BSA in MilliQ water) solution for at least 30 min at room temperature shaking at 700 rpm with a digital microplate shaker. During blocking, heat-inactivated serum samples were diluted 1:500 and 1:5,000 (IgG assay) or 1:10 and 1:100 (ACE2 assay) in diluent buffer. Each plate contained duplicates of a seven-point calibration curve with serial dilution of a reference standard, and a blank well. The plates were then washed three times with 150 µL of the MSD kit wash buffer, blotted dry, and 50 µL (IgG assay) or 25 µL (ACE2 assay) of the diluted samples were added to the plates and set to shake at 700 rpm at room temperature for at least 2 h. The plates were again washed three times and 50 µL of SULFO-Tagged anti-human IgG antibody or 25 µL of SULFO-Tagged human ACE2 protein, respectively, was added to each well and incubated shaking at 700 rpm at room temperature for at least 1 h. Plates were then washed three times and 150 µL of MSD GOLD Read Buffer B was added to each well. The plates were read immediately after on a MESO QuickPlex SQ 120 machine. Electro-chemiluminescence (ECL) signal was recorded and results expressed as AU/mL.

RBD-binding antibody ELISA

Nunc MaxiSorp high-protein-binding capacity 96-well plates (Thermo Fisher Scientific, catalog no. 44-2404-21) were coated overnight at 4°C with 1 μg/mL SARS-CoV-2 RBD diluted in phosphate-buffered saline (PBS). The next day, the plates were washed with PBS-Tween 20 0.05% (Sigma, catalog no. P2287-100ML) using the Biotek 405 TS Microplate washer. Each plate was washed five times with 200 μL of wash buffer and then dried before the next step. Following the first wash, 200 μL of Blocker Casein in PBS (Thermo Fisher Scientific, catalog no. 37528) were added to each well and incubated for 2 h at RT. After blocking, serum samples were serially diluted in blocking solution starting at 1:100 dilution. Rhesus BAL samples were added undiluted and serially diluted in blocking solution. After an hour of incubation, the plates were washed and 100 μL of secondary Peroxidase AffiniPure Rabbit Anti-Mouse IgG (Jackson ImmunoResearch, catalog no. 315-035-045, RRID: AB_2340066) antibody diluted 1:1,000 in blocking solution was added to each well. After 1 h of incubation at room temperature, the plates were washed and developed for 3.5 min with 100 μL of SeraCare SureBlue Reserve TMB Microwell Peroxidase Substrate solution (SeraCare, catalog no. 53-00-03). The reaction was then stopped with 100 μL of SeraCare KPL TMB Stop Solution (SeraCare, catalog no. 50-85-06). Optical density (OD) at 450 nm was measured using a Biotek Synergy H1 plate reader. The titer was the reciprocal of the highest dilution with absorbance values higher than four times the average of the negative control wells.

Pseudovirus neutralizing assay

This assay was performed as previously described.[33] Briefly, pseudolentiviruses were produced by triple transfection of psPAX2, pCMV-SARS2-Spike (wild type or VOC) and pCMV-Lenti-Luc in HEK293T cells. After 48 h, the supernatant of the cells was harvested, centrifuged at 4,000 rpm at 4°C for 5 min, and filtered through a 0.45-μm filter. Pseudovirus TCID50 was calculated by limiting dilution in HEK293T-ACE2 cells. For the neutralization assay, serial dilutions of sera were incubated with the pseudovirus for 45 min at 37°C, and subsequently added to HEK293T-ACE2 cells. Forty-eight hours later, luciferase signal was measured to calculate the half-maximal effective concentration (EC50) values for each serum sample.

IFN-γ and IL-4 ELISpot assay in mouse

IFN-γ and IL-4 ELISpot were performed in mouse splenocytes as previously described.[44] Briefly, 10 μg/mL anti-mouse IFN-γ ELISpot capture antibody (BD Biosciences catalog no. 551881, RRID: AB_2868948) or 4 μg/mL anti-mouse IL-4 ELISpot capture antibody (BD Biosciences catalog no. 551878, RRID: AB_2336921) were used as capture antibody. One million freshly isolated splenocytes were seeded into the precoated plates and stimulated with S1 and S2 peptides pools (GenScript) with a final concentration of 1 μg/mL of each peptide diluted in RPMI-1640 supplemented with 10% FBS and incubated for 48 h at 37°C with 5% CO_2. Each peptide pool consisted of 15-mers peptides overlapping by 10 amino acids, spanning the entire SARS-CoV-2 Spike protein S1 or S2 subunits. Control wells contained 5×10^5 cells stimulated with DMSO diluted in RPMI-1640 supplemented with 10% FBS (negative control) or 2 μg/mL concanavalin A (positive control). Subsequently, the plates were washed and incubated with biotin-conjugated mouse IFN-γ ELISpot Detection Antibody (BD Biosciences catalog no. 551881, RRID: AB_2868948) and 4 μg/mL biotin-conjugated mouse IL-4 detection antibody (BD Biosciences catalog no. 551878, RRID: AB_2336921) at room temperature for 3 h and followed by streptavidin-HRP (dilution 1:1,000, Sigma-Aldrich, catalog no. 18-152) for 45 min. After washing, 100 μL/well of NBT/BCIP substrate solution (Promega, catalog no. S3771) were added and developed for 15–30 min until distinct spots emerged. The cytokine-secreting cell spots were imaged and counted on an AID ELISpot reader (Autoimmun Diagnostika GmbH).

IFN-γ ELISpot assay in NHP PBMCs

IFNγ ELISpot assay was performed in cynomolgus macaque PBMCs using the Monkey IFNg ELISpot PRO kit (Mabtech, #3421M-2APT) according to the manufacturer's instructions. PBMCs were plated at a concentration of 200,000 cells per well and were stimulated with Wuhan or Beta SARS-CoV-2 Spike peptides (PepMix) synthetized by JPT Peptide Technologies (Berlin, Germany). These 15 mer peptides are divided in two pools (S1 and S2) of respectively 158 and 157 peptides overlapping by 11 amino acids. The peptides are coding for the S protein of SARS-CoV-2 and will be used at a final concentration of 2 μg/mL. Plates were incubated for 18 h at 37°C in an atmosphere containing 5% CO_2, then washed five times with PBS and incubated for 2 h at 37°C with a biotinylated anti-IFNγ antibody. After five washes, spots were developed by adding 0.45-mm-filtered ready-to-use BCIP/NBT-plus substrate solution and counted with an automated ELISpot reader ELRIFL04 (Autoimmun Diagnostika GmbH, Strassberg, Germany). Spot-forming units (SFU) per 10^6 PBMCs are means of duplicate wells for each stimulation and each animal.

Intracellular staining in PBMCs

T cell responses were characterized by measurement of the frequency of PBMCs expressing IL-2 (PerCP5.5, 1:10; # 560708; MQ1-17H12, BD), IL-17a (Alexa 700, 1:20; # 560613; N49-653, BD), IFN-γ (V450, 1:33.3; # 560371; B27, BD), TNF-α (BV605, 1:30.3; # 502936; Mab11, BioLegend), IL-13 (BV711, 1:20; # 564288; JES10-5A2, BD), CD137 (APC, 1:20; # 550890; 4B4, BD), and CD154 (FITC, 1:20; # 555699; TRAP1, BD) upon stimulation with the two Wuhan SARS-CoV-2 PepMix synthetized by JPT Peptide Technologies (Berlin, Germany) peptide pools. CD3 (APC-Cy7, 1:200; #557757; SP34-2, BD), CD4 (BV510, 1:33.3; # 563094; L200, BD), and CD8 (PE-Vio770, 1:50; # 130-113-159; BW135/80, Miltenyi Biotec) antibodies were used as lineage markers. One million PBMCs were cultured in complete medium (RPMI1640 Glutamax+, Gibco; supplemented with 10% FBS), supplemented with co-stimulatory antibodies (FastImmune CD28/CD49d, Becton Dickinson). Then cells were stimulated with S sequence overlapping peptide pools at a final concentration of 2 μg/mL. Brefeldin A was added to each well at a final concentration of 10 μg/mL and the plate was incubated at 37°C, 5% CO_2, for 18 h. Next, cells were washed, stained with a viability dye (LIVE/DEAD Fixable Blue Dead Cell Stain Kit, Thermo Fisher), and then fixed and permeabilized with

the BD Cytofix/Cytoperm reagent. Permeabilized cell samples were stored at −80°C before the staining procedure. Antibody staining was performed in a single step following thawing. After 30 min of incubation at 4°C, in the dark, cells were washed in BD Perm/Wash buffer then acquired on the LSRII flow cytometer (BD). Analysis was performed with FlowJo v.10 software.

SARS-CoV-2 genomic and subgenomic RNA RT-qPCR

Upper respiratory (nasopharyngeal and tracheal) specimens were collected with swabs (Viral Transport Medium, CDC, DSR-052-01). Tracheal swabs were performed by insertion of the swab above the tip of the epiglottis into the upper trachea at approximately 1.5 cm of the epiglottis. All specimens were stored between 2°C and 8°C until analysis by RT-qPCR with a plasmid standard concentration range containing an RdRp gene fragment including the RdRp-IP4 RT-PCR target sequence. The limit of detection was estimated to be 2.67 $\log_{10}$ copies of SARS-CoV-2 gRNA per milliliter and the limit of quantification was estimated to be 3.67 $\log_{10}$ copies per milliliter. SARS-CoV-2 E gene subgenomic mRNA (sgRNA) levels were assessed by RT-qPCR using primers and probes previously described:[45,46] leader-specific primer sgLeadSARSCoV2-F CGATCTCTTGTAGATCTGTTCTC, E-Sarbeco-R primer ATATTGCAGCAGTACGCACACA, and E-Sar beco probe HEX-ACACTAGCCATCCTTACTGCGCTTCG-BHQ1. The protocol describing the procedure for the detection of SARS-CoV-2 is available on the WHO website (https://www.who.int/docs/default-source/coronaviruse/real-time-rt-pcr-assays-for-the-detection-of-sars-cov-2-institut-pasteur-paris.pdf?sfvrsn=3662fcb6_2). The lim it of detection was estimated to be 2.87 $\log_{10}$ copies of SARS-CoV-2 sgRNA per milliliter, and the limit of quantification was estimated to be 3.87 $\log_{10}$ copies per milliliter.

18F-FDG PET-CT protocol

All imaging acquisitions were performed on the Digital Photon Counting (DPC) PET-CT system (Vereos-Ingenuity, Philips)[47] implemented in the BSL3 laboratory.

For imaging sessions, animals were first anesthetized with ketamine (10 mg/kg) + medetomidine (0.05mg/kg) and then maintained under isoflurane 2% in a supine position on a patient warming blanket (Bear Hugger, 3M) on the machine bed with cardiac rate, oxygen saturation, and temperature monitoring.

CT was performed under breath hold 5 min prior to PET scan for attenuation correction and anatomical localization. The CT detector collimation used was 64 × 0.6 mm, the tube voltage was 120 kV, and intensity was about 150 mAs. Automatic dose optimization tools (Dose Right, Z-DOM, 3D-DOM by Philips Healthcare) regulated the intensity. CT images were reconstructed with a slice thickness of 1.25 mm and an interval of 0.25 mm.

A whole-body PET scan (four or five bed positions, 3 min/bed position) was performed 45 min post injection of 3.39 ± 0.28 MBq/kg of 18F-fluorodeoxyglucose (FDG) via the saphenous vein. PET images were reconstructed onto a 256 × 256 matrix (three iterations, 17 subsets).

Images were analyzed using INTELLISPACE PORTAL 8 (Philips Healthcare) and 3DSlicer (open source tool). Different regions of interest (lung and lung draining lymph nodes) were defined by CT and PET. Pulmonary lesions were defined as ground glass opacity, crazy-paving pattern, or consolidation as previously described.[48–50] Lesion features detected by CT imaging were assessed by two analyzers independently and final CT score results were obtained by consensus.

Besides, regions with FDG uptake (lung, lung draining lymph nodes, and spleen) were also defined for quantification of standardized uptake value (SUV) parameters, including SUVmean and SUVmax.

Lung histopathological analysis and scoring

At necropsy, cranial and caudal lobes of the lungs were fixed by immersion in 10% formalin solution for 24 h. Samples were formalin fixed paraffin embedded (FFPE) with vacuum inclusion processor (Excelsior, Thermo) and cut in 5-µm (Microtome RM2255, Leica) slices mounted on coated glass slides (Superfrost+, Thermo) and stained with hematoxylin and eosin (H&E) with automated staining processor (Autostainer ST5020, Leica).

Each slide was scored in 20 different spots at ×40 magnification (Plan Apo λ 40×, 0.95 numerical aperture, 0.86 mm^2 per field of view). On each spot, five different parameters were assessed: septal cellularity, septal fibrosis, type II pneumocytes, hyperplasia, and alveolar neutrophils. A systematic histopathology scoring was used and is described in Table S1. Each score were then calculated for each assessed field of view for cranial and caudal lobes.

Biodistribution/gene expression studies

Tissue collection was segregated for genomic DNA (gDNA) or total RNA work by QIASymphony nucleic acid extraction with the aim of filling up 96-well plates of purified material. A small cut of frozen tissue (∼20 mg) was used for all extractions with the exception of gDNA purifications from spleen (1–2 mg). Tissues were disrupted and homogenized in QIAGEN Buffer ATL (180 µL) and lysed overnight at 56°C in the presence of QIAGEN Proteinase K (400 µg) for gDNA, or directly in QIAGEN Buffer RLT-Plus in the presence of 2-mercaptoethanol and a QIAGEN anti-foaming agent for total RNA purification. Tissue lysates for gDNA extraction were treated in advance with QIAGEN RNase A (400 µg), while tissue homogenates for RNA extraction were DNase-I treated *in situ* in the QIASymphony during the procedure. Nucleic acids were quantified only if necessary, as a troubleshooting measure. Purified gDNA samples were diluted 10-fold and in parallel into Cutsmart-buffered BamHI-HF (New England Biolabs) restriction digestions in the presence of 0.1% Pluronic F-68 (50µL final volume) that ran overnight prior to quantification. Similarly, DNase-I-treated total RNAs were diluted 10-fold into cDNA synthesis reactions (20 µL final volume) with or without reverse transcriptase using the High Capacity cDNA Reverse Transcription Kit (Thermo Fisher). For ddPCR

(gDNA or cDNA) or qPCR (cDNA), 2 μL of processed nucleic acids were used for quantification using Bio-Rad or Applied Biosystems reagents, respectively, in 20-μL reactions using default amplification parameters without an UNG incubation step. All the studies included negative control (PBS) groups for comparison. The significantly small variance of multiple technical replicates in ddPCR justified the use of a single technical replicate per sample and no less than three biological replicates per group, gender, or time point. coRBD signal for ddPCR and vector biodistribution (gDNA) was multiplexed and normalized against the mouse transferrin receptor (Tfrc) gene TaqMan assay using a commercial preparation validated for copy number variation analysis (Thermo Fisher Scientific). Likewise, coRBD signal for ddPCR and gene expression analysis was multiplexed and normalized against the mouse GAPDH gene, also using a commercial preparation of the reference assay (Thermo Fisher Scientific). Target and reference oligonucleotide probes are tagged with different fluorophores at the 5′ end, which allows efficient signal stratification. For qPCR, coRBD and mGAPDH TaqMan assays were run separately to minimize competitive PCR multiplexing issues prior to analysis and delta delta Ct normalization.[51] The limit of detection of the assay was 10 copies/reaction; therefore, wells with fewer than 10 copies were considered negative.

Statistical analysis

GraphPad Prism 9 was used for graph preparation and statistical analysis. Groups were compared between them by Kruskal Wallis and Dunn's test. Two groups were compared between them using Student's t test (independent samples, $n \geq 10$) and Mann-Whitney's U (independent samples, $n < 10$).

SUPPLEMENTAL INFORMATION

Supplemental information can be found online at https://doi.org/10.1016/j.ymthe.2022.05.007.

ACKNOWLEDGMENTS

We thank the Bill and Melinda Gates Foundation for funding the NHP challenge studies. These studies would not have been possible without the responsiveness and help of dozens of individuals within Mass Eye and Ear, Mass General, Mass General Brigham Innovation, the Gene Therapy Program at the University of Pennsylvania, Novartis Gene Therapies, Novartis Institutes for Biomedical Research, the Penn Center for Innovation, 5AM Ventures, Aldevron, and Catalent. We thank A. Sheridan from the Grousbeck Center Gene Transfer Vector Core at Mass Eye and Ear for AAV production; C. Leborgne from Genethon for anti-AAV Nab prescreen in NHP; and N. Hacohen and M. Gentili from the Broad Institute for providing pseudovirus reagents. We thank B. Delache, R. Ho-Tsong Fang, S. Langlois, Q. Sconosciuti, V. Magneron, P. Le Calvez, M. Potier, J. M. Robert, N. Dhooge, T. Prot, and C. Dodan for the NHP experiments; L. Bossevot, M. Leonec, L. Moenne-Loccoz, M. Galpin-Lebreau, L. Pintore, and J. Morin for the RT-qPCR, ELISpot, and MSD serology assays, and for the preparation of reagents; W. Gros, J. Van Wassenhove, and M Gomez-Pacheco for NHP T-cell assays and intracellular staining as well as analysis; C. Chapon for imagery analysis; and S. Luccantoni and C. Ludot for histology sample preparation. We thank the R&D platform with R. Marlin, M. Galhaut, N. Dimant, and V. Contreras for scientific discussion and help; M. Barendji, J. Dinh, and E. Guyon for the NHP sample processing; S. Keyser for the transport organization; F. Ducancel, A. Pouget, and Y. Gorin for their help with the logistics and safety management; and I. Mangeot and C. Morice for help with resources management. B. Targat contributed to data management. We thank S. Van der Werf, S. Bellil, and V. Enouf for contributions to viral stock challenge production; and A. Nougairede for sharing the plasmid used for the sgRNA assays standardization. The IDMIT research infrastructure is supported by the Programme Investissements d'Avenir, managed by the ANR under reference ANR-11-INBS-0008. The Fondation Bettencourt Schueller and the Region Ile-de-France contributed to the implementation of IDMIT's facilities and imaging technologies. The NHP model of SARS-CoV-2 infection has been developed thanks to the support from REACTing, the Fondation pour la Recherche Medicale (FRM; AM-CoV-Path), and the European Infrastructure TRANSVAC2 (730964). The virus stock used in NHPs was obtained through the EVAg platform (https://www.european-virus-archive.com/), funded by H2020 (653316) or from the Biodefense, Research Resources, and Translational Research of NIH/NIAID/DMID/OBRRTR/RRS (Program Officer, Clint Florence, PhD). Funding for this project was provided by donations from Giving/Grousbeck (Emilia Fazzalari and Wyc Grousbeck) and multiple other donors (Nathalie, Alexandre, and Charles de Gunzburg; David Vargo; Julia and Mark Casady and the One Step Forward Education Foundation; Katrine S. Bosley; Tamra Gould and Howard Amster II Donor Advised Fund of the Jewish Federation of Cleveland; The Tej Kohli Foundation; Michel Plantevin; Susan Stoddart and Chris Snook; Delori Family; Annette and Dan Nova; Jennifer and Jonathan Uhrig; Lyle Howland and Jack Manning; Michelle and Bob Atchinson; Elizabeth and Phill Gross; William and Carolyn Aliski) through the Mass Eye and Ear donor network (L.H.V.); grants from the Massachusetts Consortium for Pathogen Readiness and Mark and Lisa Schwartz (L.H.V.); George Mason University Fast Grants; the Bill and Melinda Gates Foundation (L.H.V.), Sponsored Research Agreements from Albamunity (L.H.V) and an in-kind donation of AAV manufacturing services and product by Novartis Gene Therapies.

AUTHOR CONTRIBUTIONS

Conceptualization, N.Z., U.B., C.H., P.M., R.L.G., J.M.W. and L.H.V.; methodology, N.Z., U.B., C.H., P.M., J.S., N.D.-B., T.N., Q.P., J.L., G.R., E.M., F.R., R.L.G., and L.H.V.; validation, N.Z., U.B., and C.H.; formal analysis, N.Z., C.H., P.M., N.D.-B., M.C., Q.P., A-S.G., T.N., N.K., R.L.G., and L.H.V.; investigation, N.Z., U.B., J.S., R.E., C.D., S.C., D.L., C.H., P.M., N.D.-B., M.C., A.-S.G., T.N., N.K., and C.C.; resources, J.L., F.R., G.R., H.J.T., E.M., R.L.G., and L.H.V.; writing – original draft, N.Z., U.B., and L.H.V.; writing – review & editing, N.Z., U.B., C.H., P.M., J.S., R.L.G., and L.H.V.; visualization, N.Z., U.B., and C.H.; supervision, N.Z., C.H., R.L.G., J.M.W. and L.H.V.; project administration, N.Z., C.H., and P.M; funding acquisition, R.L.G. and L.H.V.

DECLARATION OF INTERESTS

J.M.W. is a paid advisor to and holds equity in Scout Bio and Passage Bio; he holds equity in Surmount Bio; he also has sponsored research agreements with Amicus Therapeutics, Biogen, Elaaj Bio, Janssen, Moderna, Passage Bio, Regeneron, Scout Bio, Surmount Bio, and Ultragenyx, which are licensees of Penn technology. L.H.V. and J.M.W. are inventors on patents that have been licensed to various biopharmaceutical companies and for which they may receive payments. L.H.V. is a paid advisor to Novartis, Akouos, and Affinia Therapeutics and serves on the Board of Directors of Affinia, Addgene, and Odylia Therapeutics. L.H.V. holds equity in Akouos and Affinia and receives sponsored research funding from Albamunity, to which he is an unpaid consultant. L.H.V. is co-founder and an employee of Ciendias Bio, a biotechnology company that pursues the development of AAV-based vaccines. L.H.V. further is a listed inventor on various gene transfer technologies, including some relevant to AAVCOVID. L.H.V. is a scientific advisory board member to Akouos, and board member of Affinia Therapeutics, companies of which he is a co-founder. U.B., N.Z. and L.H.V. are listed inventors on several patent applications on the described technologies.

REFERENCES

1. Baden, L.R., El Sahly, H.M., Essink, B., Kotloff, K., Frey, S., Novak, R., Diemert, D., Spector, S.A., Rouphael, N., Creech, C.B., et al. (2021). Efficacy and safety of the mRNA-1273 SARS-CoV-2 vaccine. New Engl. J. Med. *384*, 403–416. https://doi.org/10.1056/NEJMoa2035389.
2. Polack, F.P., Thomas, S.J., Kitchin, N., Absalon, J., Gurtman, A., Lockhart, S., Perez, J.L., Perez Marc, G., Moreira, E.D., Zerbini, C., et al. (2020). Safety and efficacy of the BNT162b2 mRNA Covid-19 vaccine. New Engl. J. Med. *383*, 2603–2615. https://doi.org/10.1056/NEJMoa2034577.
3. Heath, P.T., Galiza, E.P., Baxter, D.N., Boffito, M., Browne, D., Burns, F., Chadwick, D.R., Clark, R., Cosgrove, C., Galloway, J., et al. (2021). Safety and efficacy of NVX-CoV2373 Covid-19 vaccine. New Engl. J. Med. *385*, 1172–1183. https://doi.org/10.1056/NEJMoa2107659.
4. Sadoff, J., Gray, G., Vandebosch, A., Cardenas, V., Shukarev, G., Grinsztejn, B., Goepfert, P.A., Truyers, C., Fennema, H., Spiessens, B., et al. (2021). Safety and efficacy of single-dose Ad26.COV2.S vaccine against Covid-19. New Engl. J. Med. *384*, 2187–2201. https://doi.org/10.1056/NEJMoa2101544.
5. Andrews, N., Tessier, E., Stowe, J., Gower, C., Kirsebom, F., Simmons, R., Gallagher, E., Thelwall, S., Groves, N., Dabrera, G., et al. (2022). Duration of protection against mild and severe disease by Covid-19 vaccines. N. Engl. J. Med. *386*, 340–350. https://doi.org/10.1056/NEJMoa2115481.
6. Pegu, A., O'Connell, S.E., Schmidt, S.D., O'Dell, S., Talana, C.A., Lai, L., Albert, J., Anderson, E., Bennett, H., Corbett, K.S., et al. (2021). Durability of mRNA-1273 vaccine-induced antibodies against SARS-CoV-2 variants. Science *373*, 1372–1377. https://doi.org/10.1126/science.abj4176.
7. Collier, A.r.Y., Yu, J., McMahan, K., Liu, J., Chandrashekar, A., Maron, J.S., Atyeo, C., Martinez, D.R., Ansel, J.L., Aguayo, R., et al. (2021). Differential kinetics of immune responses elicited by Covid-19 vaccines. New Engl. J. Med. *385*, 2010–2012. https://doi.org/10.1056/NEJMc2115596.
8. Gagne, M., Corbett, K.S., Flynn, B.J., Foulds, K.E., Wagner, D.A., Andrew, S.F., Todd, J.P.M., Honeycutt, C.C., McCormick, L., Nurmukhambetova, S.T., et al. (2021). Protection from SARS-CoV-2 Delta one year after mRNA-1273 vaccination in nonhuman primates is coincident with an anamnestic antibody response in the lower airway. Preprint at bioRxiv. https://doi.org/10.1101/2021.10.23.465542.
9. Singanayagam, A., Hakki, S., Dunning, J., Madon, K.J., Crone, M.A., Koycheva, A., Derqui-Fernandez, N., Barnett, J.L., Whitfield, M.G., Varro, R., et al. (2022). Community transmission and viral load kinetics of the SARS-CoV-2 delta (B.1.617.2) variant in vaccinated and unvaccinated individuals in the UK: a prospective, longitudinal, cohort study. Lancet Infect. Dis. *22*, 183–195. https://doi.org/10.1016/S1473-3099(21)00648-4.
10. Korber, B., Fischer, W.M., Gnanakaran, S., Yoon, H., Theiler, J., Abfalterer, W., Hengartner, N., Giorgi, E.E., Bhattacharya, T., Foley, B., et al. (2020). Tracking changes in SARS-CoV-2 spike: evidence that D614G increases infectivity of the COVID-19 virus. Cell *182*, 812–827.e19. https://doi.org/10.1016/j.cell.2020.06.043.
11. Garcia-Beltran, W.F., Lam, E.C., Astudillo, M.G., Yang, D., Miller, T.E., Feldman, J., Hauser, B.M., Caradonna, T.M., Clayton, K.L., Nitido, A.D., et al. (2021). COVID-19-neutralizing antibodies predict disease severity and survival. Cell *184*, 476–488.e11. https://doi.org/10.1016/j.cell.2020.12.015.
12. Legros, V., Denolly, S., Vogrig, M., Boson, B., Siret, E., Rigaill, J., Pillet, S., Grattard, F., Gonzalo, S., Verhoeven, P., et al. (2021). A longitudinal study of SARS-CoV-2-infected patients reveals a high correlation between neutralizing antibodies and COVID-19 severity. Cell Mol. Immunol. *18*, 318–327. https://doi.org/10.1038/s41423-020-00588-2.
13. Volz, E., Mishra, S., Chand, M., Barrett, J.C., Geidelberg, L., Hinsley, W.R., Dabrera, G., O'Toole, Á., Ragonnet-Cronin, M., Harrison, I., et al. (2021). Assessing transmissibility of SARS-CoV-2 lineage B.1.1.7 in England. Nature *593*, 266–269. https://doi.org/10.1038/s41586-021-03470-x.
14. Tegally, H., Wilkinson, E., Giovanetti, M., Iranzadeh, A., Fonseca, V., Giandhari, J., Doolabh, D., Pillay, S., San, E.J., Msomi, N., et al. (2021). Detection of a SARS-CoV-2 variant of concern in South Africa. Nature *592*, 438–443. https://doi.org/10.1038/s41586-021-03402-9.
15. Faria, N.R., Mellan, T.A., Whittaker, C., Claro, I.M., Candido, D.D.S., Mishra, S., Crispim, M.A.E., Sales, F.C.S., Hawryluk, I., McCrone, J.T., et al. (2021). Genomics and epidemiology of the P.1 SARS-CoV-2 lineage in Manaus, Brazil. Science *372*, 815–821. https://doi.org/10.1126/science.abh2644.
16. Naveca, F.G., Nascimento, V., de Souza, V.C., Corado, A.d.L., Nascimento, F., Silva, G., Costa, A., Duarte, D., Pessoa, K., Mejia, M., et al. (2021). COVID-19 in Amazonas, Brazil, was driven by the persistence of endemic lineages and P.1 emergence. Nat. Med. *27*, 1230–1238. https://doi.org/10.1038/s41591-021-01378-7.
17. Cherian, S., Potdar, V., Jadhav, S., Yadav, P., Gupta, N., Das, M., Rakshit, P., Singh, S., Abraham, P., Panda, S., and Team, N. (2021). SARS-CoV-2 spike mutations, L452R, T478K, E484Q and P681R, in the second wave of COVID-19 in Maharashtra, India. Microorganisms *9*, 1542. https://doi.org/10.3390/microorganisms9071542.
18. Garcia-Beltran, W.F., Lam, E.C., St Denis, K., Nitido, A.D., Garcia, Z.H., Hauser, B.M., Feldman, J., Pavlovic, M.N., Gregory, D.J., Poznansky, M.C., et al. (2021). Multiple SARS-CoV-2 variants escape neutralization by vaccine-induced humoral immunity. Cell *184*, 2523. https://doi.org/10.1016/j.cell.2021.04.006.
19. Zhou, D., Dejnirattisai, W., Supasa, P., Liu, C., Mentzer, A.J., Ginn, H.M., Zhao, Y., Duyvesteyn, H.M.E., Tuekprakhon, A., Nutalai, R., et al. (2021). Evidence of escape of SARS-CoV-2 variant B.1.351 from natural and vaccine-induced sera. Cell *184*, 2348–2361.e6. https://doi.org/10.1016/j.cell.2021.02.037.
20. Hoffmann, M., Arora, P., Groß, R., Seidel, A., Hornich, B.F., Hahn, A.S., Kruger, N., Graichen, L., Hofmann-Winkler, H., Kempf, A., et al. (2021). SARS-CoV-2 variants B.1.351 and P.1 escape from neutralizing antibodies. Cell *184*, 2384–2393.e12. https://doi.org/10.1016/j.cell.2021.03.036.
21. Planas, D., Veyer, D., Baidaliuk, A., Staropoli, I., Guivel-Benhassine, F., Rajah, M.M., Planchais, C., Porrot, F., Robillard, N., Puech, J., et al. (2021). Reduced sensitivity of SARS-CoV-2 variant Delta to antibody neutralization. Nature *596*, 276–280. https://doi.org/10.1038/s41586-021-03777-9.
22. Collier, D.A., De Marco, A., Ferreira, I., Meng, B., Datir, R., Walls, A.C., Kemp, S.S., Bassi, J., Pinto, D., Fregni, C.S., et al. (2021). SARS-CoV-2 B.1.1.7 sensitivity to mRNA vaccine-elicited, convalescent and monoclonal antibodies. Preprint at medRxiv. https://doi.org/10.1101/2021.01.19.21249840.
23. Emary, K.R.W., Golubchik, T., Aley, P.K., Ariani, C.V., Angus, B., Bibi, S., Blane, B., Bonsall, D., Cicconi, P., Charlton, S., et al. (2021). Efficacy of ChAdOx1 nCoV-19 (AZD1222) vaccine against SARS-CoV-2 variant of concern 202012/01 (B.1.1.7): an exploratory analysis of a randomised controlled trial. Lancet *397*, 1351–1362. https://doi.org/10.1016/S0140-6736(21)00628-0.
24. Wibmer, C.K., Ayres, F., Hermanus, T., Madzivhandila, M., Kgagudi, P., Oosthuysen, B., Lambson, B.E., de Oliveira, T., Vermeulen, M., van der Berg, K., et al. (2021).

SARS-CoV-2 501Y.V2 escapes neutralization by South African COVID-19 donor plasma. Nat. Med. *27*, 622–625. https://doi.org/10.1038/s41591-021-01285-x.

25. Yu, J., Tostanoski, L.H., Mercado, N.B., McMahan, K., Liu, J., Jacob-Dolan, C., Chandrashekar, A., Atyeo, C., Martinez, D.R., Anioke, T., et al. (2021). Protective efficacy of Ad26.COV2.S against SARS-CoV-2 B.1.351 in macaques. Nature *596*, 423–427. https://doi.org/10.1038/s41586-021-03732-8.

26. Corbett, K.S., Werner, A.P., S, O.C., Gagne, M., Lai, L., Moliva, J.I., Flynn, B., Choi, A., Koch, M., Foulds, K.E., et al. (2021). Evaluation of mRNA-1273 against SARS-CoV-2 B.1.351 infection in nonhuman primates. bioRxiv. Preprint at. https://doi.org/10.1101/2021.05.21.445189.

27. Mlcochova, P., Kemp, S.A., Dhar, M.S., Papa, G., Meng, B., Ferreira, I.A.T.M., Datir, R., Collier, D.A., Albecka, A., Singh, S., et al.; The Indian SARS-CoV-2 Genomics Consortium INSACOG; The Genotype to Phenotype Japan G2P-Japan Consortium; The CITIID-NIHR BioResource COVID-19 Collaboration (2021). SARS-CoV-2 B.1.617.2 Delta variant replication and immune evasion. Nature *599*, 114–119. https://doi.org/10.1038/s41586-021-03944-y.

28. Mizrahi, B., Lotan, R., Kalkstein, N., Peretz, A., Perez, G., Ben-Tov, A., Chodick, G., Gazit, S., and Patalon, T. (2021). Correlation of SARS-CoV-2-breakthrough infections to time-from-vaccine. Nat. Commun. *12*, 6379. https://doi.org/10.1038/s41467-021-26672-3.

29. Planas, D., Saunders, N., Maes, P., Guivel-Benhassine, F., Planchais, C., Buchrieser, J., Bolland, W.H., Porrot, F., Staropoli, I., Lemoine, F., et al. (2022). Considerable escape of SARS-CoV-2 Omicron to antibody neutralization. Nature *602*, 671–675. https://doi.org/10.1038/s41586-021-04389-z.

30. Garcia-Beltran, W.F., St Denis, K.J., Hoelzemer, A., Lam, E.C., Nitido, A.D., Sheehan, M.L., Berrios, C., Ofoman, O., Chang, C.C., Hauser, B.M., et al. (2022). mRNA-based COVID-19 vaccine boosters induce neutralizing immunity against SARS-CoV-2 Omicron variant. Cell *185*, 457–466.e4. https://doi.org/10.1016/j.cell.2021.12.033.

31. Barouch, D.H., Stephenson, K.E., Sadoff, J., Yu, J., Chang, A., Gebre, M., McMahan, K., Liu, J., Chandrashekar, A., Patel, S., et al. (2021). Durable humoral and cellular immune responses 8 Months after Ad26.COV2.S vaccination. New Engl. J. Med. *385*, 951–953. https://doi.org/10.1056/NEJMc2108829.

32. Gagne, M., Moliva, J.I., Foulds, K.E., Andrew, S.F., Flynn, B.J., Werner, A.P., Wagner, D.A., Teng, I.-T., Lin, B.C., Moore, C., et al. (2022). mRNA-1273 or mRNA-Omicron boost in vaccinated macaques elicits comparable B cell expansion, neutralizing antibodies and protection against Omicron. Preprint at bioRxiv. https://doi.org/10.1101/2022.02.03.479037.

33. Zabaleta, N., Dai, W., Bhatt, U., Herate, C., Maisonnasse, P., Chichester, J.A., Sanmiguel, J., Estelien, R., Michalson, K.T., Diop, C., et al. (2021). An AAV-based, room-temperature-stable, single-dose COVID-19 vaccine provides durable immunogenicity and protection in non-human primates. Cell Host Microbe *29*, 1437–1453.e8. https://doi.org/10.1016/j.chom.2021.08.002.

34. Lescure, F.X., Bouadma, L., Nguyen, D., Parisey, M., Wicky, P.H., Behillil, S., Gaymard, A., Bouscambert-Duchamp, M., Donati, F., Le Hingrat, Q., et al. (2020). Clinical and virological data of the first cases of COVID-19 in Europe: a case series. Infect. Dis. *20*, 697–706. https://doi.org/10.1016/S1473-3099(20)30200-0.

35. Mori, S., Wang, L., Takeuchi, T., and Kanda, T. (2004). Two novel adeno-associated viruses from cynomolgus monkey: pseudotyping characterization of capsid protein. Virology *330*, 375–383. https://doi.org/10.1016/j.virol.2004.10.012.

36. Vandenberghe, L.H., Breous, E., Nam, H.J., Gao, G., Xiao, R., Sandhu, A., Johnston, J., Debyser, Z., Agbandje-McKenna, M., and Wilson, J.M. (2009). Naturally occurring singleton residues in AAV capsid impact vector performance and illustrate structural constraints. Gene Ther. *16*, 1416–1428. https://doi.org/10.1038/gt.2009.101.

37. Mietzsch, M., Jose, A., Chipman, P., Bhattacharya, N., Daneshparvar, N., McKenna, R., and Agbandje-McKenna, M. (2021). Completion of the AAV structural Atlas: serotype capsid structures reveals Clade-specific features. Viruses *13*, 101. https://doi.org/10.3390/v13010101.

38. Grieger, J.C., and Samulski, R.J. (2005). Packaging capacity of adeno-associated virus serotypes: impact of larger genomes on infectivity and postentry steps. J. Virol. *79*, 9933–9944. https://doi.org/10.1128/JVI.79.15.9933-9944.2005.

39. Wu, Z., Yang, H., and Colosi, P. (2010). Effect of genome size on AAV vector packaging. Mol. Ther. *18*, 80–86. https://doi.org/10.1038/mt.2009.255.

40. Moyo-Gwete, T., Madzivhandila, M., Makhado, Z., Ayres, F., Mhlanga, D., Oosthuysen, B., Lambson, B.E., Kgagudi, P., Tegally, H., Iranzadeh, A., et al. (2021). Cross-reactive neutralizing antibody responses elicited by SARS-CoV-2 501Y.V2 (B.1.351). New Engl. J. Med. *384*, 2161–2163. https://doi.org/10.1056/NEJMc2104192.

41. Liu, C., Ginn, H.M., Dejnirattisai, W., Supasa, P., Wang, B., Tuekprakhon, A., Nutalai, R., Zhou, D., Mentzer, A.J., Zhao, Y., et al. (2021). Reduced neutralization of SARS-CoV-2 B.1.617 by vaccine and convalescent serum. Cell *184*, 4220–4236.e13. https://doi.org/10.1016/j.cell.2021.06.020.

42. Morens, D.M., Taubenberger, J.K., and Fauci, A.S. (2022). Universal coronavirus vaccines - an urgent need. New Engl. J. Med. *386*, 297–299. https://doi.org/10.1056/NEJMp2118468.

43. Johnson, M., Wagstaffe, H.R., Gilmour, K.C., Mai, A.L., Lewis, J., Hunt, A., Sirr, J., Bengt, C., Grandjean, L., and Goldblatt, D. (2020). Evaluation of a novel multiplexed assay for determining IgG levels and functional activity to SARS-CoV-2. J. Clin. Virol. *130*, 104572. https://doi.org/10.1016/j.jcv.2020.104572.

44. Wang, X., Yan, Y., Gan, T., Yang, X., Li, D., Zhou, D., Sun, Q., Huang, Z., and Zhong, J. (2019). A trivalent HCV vaccine elicits broad and synergistic polyclonal antibody response in mice and rhesus monkey. Gut *68*, 140–149. https://doi.org/10.1136/gutjnl-2017-314870.

45. Corman, V.M., Landt, O., Kaiser, M., Molenkamp, R., Meijer, A., Chu, D.K., Bleicker, T., Brunink, S., Schneider, J., Schmidt, M.L., et al. (2020). Detection of 2019 novel coronavirus (2019-nCoV) by real-time RT-PCR. Euro Surveill. *25*, 2000045. https://doi.org/10.2807/1560-7917.ES.2020.25.3.2000045.

46. Wolfel, R., Corman, V.M., Guggemos, W., Seilmaier, M., Zange, S., Muller, M.A., Niemeyer, D., Jones, T.C., Vollmar, P., Rothe, C., et al. (2020). Virological assessment of hospitalized patients with COVID-2019. Nature *581*, 465–469. https://doi.org/10.1038/s41586-020-2196-x.

47. Zhang, J., Binzel, K., Miller, M., Wright, C., Siva, A., Saif, T., Knopp, M., Maniawski, P., Tung, C.-h., and Knopp, M. (2016). Digital Photon counting PET/CT: the physics powering precision nuclear medicine. J. Nucl. Med. *57*, 1286.

48. Shi, H., Han, X., Jiang, N., Cao, Y., Alwalid, O., Gu, J., Fan, Y., and Zheng, C. (2020). Radiological findings from 81 patients with COVID-19 pneumonia in Wuhan, China: a descriptive study. Lancet Infect. Dis. *20*, 425–434. https://doi.org/10.1016/S1473-3099(20)30086-4.

49. Pan, F., Ye, T., Sun, P., Gui, S., Liang, B., Li, L., Zheng, D., Wang, J., Hesketh, R.L., Yang, L., and Zheng, C. (2020). Time Course of lung changes at chest CT during recovery from coronavirus disease 2019 (COVID-19). Radiology *295*, 715–721. https://doi.org/10.1148/radiol.2020200370.

50. Maisonnasse, P., Guedj, J., Contreras, V., Behillil, S., Solas, C., Marlin, R., Naninck, T., Pizzorno, A., Lemaitre, J., Goncalves, A., et al. (2020). Hydroxychloroquine use against SARS-CoV-2 infection in non-human primates. Nature *585*, 584–587. https://doi.org/10.1038/s41586-020-2558-4.

51. Livak, K., and Schmittgen, T. (2001). Analysis of relative gene expression data using real-time quantitative PCR and the 2(-Delta Delta C(T)) Method. Methods (San Diego, Calif.) *25*, 402–408. https://doi.org/10.1006/meth.2001.1262.